Influence of neighboring modules on the thermal performance of a 2S module for the CMS Phase-2 upgrade

von
Stella Israel

Bachelorarbeit in Physik

vorgelegt der
Fakultät für Mathematik, Informatik und Naturwissenschaften der RWTH Aachen

im Mai, 2024

angefertigt im
I. Physikalischen Institut B

bei
Prüfer: Prof. Dr. Lutz Feld
Zweitprüfer: Prof. Dr. Oliver Pooth

Zentrales Prüfungsamt/Central Examination Office

Eidesstattliche Versicherung
Statutory Declaration in Lieu of an Oath

Name, Vorname/Last Name, First Name

Matrikelnummer (freiwillige Angabe)
Matriculation No. (optional)

Ich versichere hiermit an Eides Statt, dass ich die vorliegende Arbeit/Bachelorarbeit/ Masterarbeit* mit dem Titel
I hereby declare in lieu of an oath that I have completed the present paper/Bachelor thesis/Master thesis* entitled

selbstständig und ohne unzulässige fremde Hilfe (insbes. akademisches Ghostwriting) erbracht habe. Ich habe keine anderen als die angegebenen Quellen und Hilfsmittel benutzt. Für den Fall, dass die Arbeit zusätzlich auf einem Datenträger eingereicht wird, erkläre ich, dass die schriftliche und die elektronische Form vollständig übereinstimmen. Die Arbeit hat in gleicher oder ähnlicher Form noch keiner Prüfungsbehörde vorgelegen.
independently and without illegitimate assistance from third parties (such as academic ghostwriters). I have used no other than the specified sources and aids. In case that the thesis is additionally submitted in an electronic format, I declare that the written and electronic versions are fully identical. The thesis has not been submitted to any examination body in this, or similar, form.

Ort, Datum/City, Date

Unterschrift/Signature

*Nichtzutreffendes bitte streichen

*Please delete as appropriate

Belehrung:
Official Notification:

§ 156 StGB: Falsche Versicherung an Eides Statt
Wer vor einer zur Abnahme einer Versicherung an Eides Statt zuständigen Behörde eine solche Versicherung falsch abgibt oder unter Berufung auf eine solche Versicherung falsch aussagt, wird mit Freiheitsstrafe bis zu drei Jahren oder mit Geldstrafe bestraft.
Para. 156 StGB (German Criminal Code): False Statutory Declarations
Whoever before a public authority competent to administer statutory declarations falsely makes such a declaration or falsely testifies while referring to such a declaration shall be liable to imprisonment not exceeding three years or a fine.
§ 161 StGB: Fahrlässiger Falscheid; fahrlässige falsche Versicherung an Eides Statt
(1) Wenn eine der in den §§ 154 bis 156 bezeichneten Handlungen aus Fahrlässigkeit begangen worden ist, so tritt Freiheitsstrafe bis zu einem Jahr oder Geldstrafe ein.
(2) Straflosigkeit tritt ein, wenn der Täter die falsche Angabe rechtzeitig berichtigt. Die Vorschriften des § 158 Abs. 2 und 3 gelten entsprechend.
Para. 161 StGB (German Criminal Code): False Statutory Declarations Due to Negligence
(1) If a person commits one of the offences listed in sections 154 through 156 negligently the penalty shall be imprisonment not exceeding one year or a fine.
(2) The offender shall be exempt from liability if he or she corrects their false testimony in time. The provisions of section 158 (2) and (3) shall apply accordingly.

Die vorstehende Belehrung habe ich zur Kenntnis genommen:
I have read and understood the above official notification:

Ort, Datum/City, Date

Unterschrift/Signature

Contents

1. Introduction **1**

2. The LHC and the CMS Experiment **3**
2.1. The Large Hadron Collider (LHC) 3
2.2. The CMS (Compact Muon Solenoid) experiment 4
2.3. The High Luminosity LHC 5
2.3.1. The CMS Phase-2 tracker upgrade 6

3. The 2S module **9**
3.1. Design of the 2S module 9
3.2. Thermal runaway 10

4. Setup **13**
4.1. Mini-TEDD structure 14
4.2. Thermistors and heating resistors 16
4.2.1. Gluing of temperature sensors onto the carbon fiber surface 16
4.2.2. Mounting of heating resistors on remaining module positions 16
4.3. Module cooling box and CO_2 cooling system 18
4.3.1. Determination of the CO_2 temperature in a comparison of methods 19
4.4. Generation of leakage current 21

5. Measurement of the thermal runaway for the Ultimate@800V scenario with long inserts **23**
5.1. Motivation 23
5.2. Thermal runaway measurement for one 2S module on long inserts . 23
5.2.1. General measurement procedure 23
5.2.2. Results of the thermal runaway measurement of the 2S module 24
5.2.3. Comparison to short inserts 26
5.2.4. Comparison to thermal simulation 28
5.3. Effect of five neighboring modules on the thermal behavior of the cooling structure and the 2S module 29
5.4. Results of the thermal runaway measurement for the 2S module and neighboring modules 32
5.4.1. Results of the thermal runaway measurement 32
5.4.2. Comparison to 2S module on long inserts and simulation data 33

6. Investigation of the heat flux on the cooling structure **35**
6.1. Motivation 35
6.2. Results and comparison of one module powered on the top/bottom center position 35
6.3. Results and comparison of the heat flux on the carbon fiber center . 39

7. Summary **43**

References **45**

A. Appendix **47**
A.1. CO_2 cooling setup 47
A.2. Systematic uncertainty of the PT100 sensors 49
A.3. Heat distribution of the mini-TEDD structure in two configurations 50

1. Introduction

The Standard Model (SM) of particle physics summarizes the essence of particle physics today, and its predictions have been confirmed in experiments with particle accelerators. Only in 2012, the latest addition to the SM has been discovered – the Higgs Boson. It was found in the CMS and ATLAS experiments of the Large Hadron Collider (LHC) at CERN [1, 2]. The LHC is going to be upgraded into the High Luminosity LHC, that is expected to start operating in 2029. It is expected to collect 3000 - 4000 fb^{-1} of integrated luminosity during its lifespan of ten years, and reach instantaneous luminosities of 5 - 7.5 $\times$ 10^{34} $\mathrm{cm}^{-2}\,\mathrm{s}^{-1}$[3]. The tracker is a subdetector of the CMS detector and will be entirely replaced, to keep up with the requirements of the new accelerator. Therefore a strip silicon module has been developed for the new Outer Tracker, called the 2S module. It consists of two silicon sensors stacked on top of each other. The measured hits on both sensors are used to reconstruct the trajectories of charged particles and to determine their transverse momentum p_T. Information about tracks with high p_T is provided to the Level-1 trigger of CMS. The silicon sensors of the 2S module are sensitive to irradiation, which can cause a significant increase of leakage current. The leakage current of the silicon sensor is exponentially dependent on the sensor temperature. Without sufficient cooling, a 2S module can potentially enter thermal runaway, an uncontrollable self heating loop of the silicon sensors [3].
For cooling purposes, a new evaporative CO_2 cooling system is used [3]. To confirm previous simulations for the thermal runaway, the onset of thermal runaway has to be investigated in an experiment. In this thesis, a 2S module with six cooling contacts and a sensor spacing of 4 mm, and five neighboring modules, emulated by heating resistors, are mounted on a small test cooling structure. The start of the thermal runaway is investigated for ultimate performance scenario with 4000 fb^{-1} of integrated luminosity.
In Section 2 the LHC and the CMS experiment are described, as well as the planned HL-LHC with focus on the Phase-2 tracker upgrade. Section 3 describes the 2S module design and the cooling system. The setup is explained in Section 4, together with two calibration measurements regarding the CO_2 temperature measurement and current induced on the sensor by LED strips. Section 5 covers the results of the thermal runaway measurements for the 2S module mounted on long cooling contacts of the test cooling structure, and with emulated neighboring modules. In Section 6, further heat flux investigations are depicted for the test cooling structure and Section 7 summarizes the results of this thesis.

2. The LHC and the CMS Experiment

2.1. The Large Hadron Collider (LHC)

The Large Hadron Collider (LHC) is the world's largest high energy particle accelerator, located at the European Organization for Nuclear Research (CERN) at the border of Switzerland and France near Geneva. In colliding-beam experiments, the fundamental matter of the universe is explored. Therefore, the LHC accelerates protons and heavy ions; the particle collisions can even recreate about the energy density of the early universe after the Big Bang.
The LHC synchrotron has a circumference of 26.7 km and is located 100 m underground. Powerful dipole magnets alongside the ring create a strong magnetic field in excess of 8 T, to bend the particles in the circular direction of the ring, while radiofrequency cavities accelerate the particles [4, 5]. The large size of the ring accomplishes the acceleration of particles to particularly high energies. The high bunch population with about 10^{11} protons per bunch, the high bunch frequency inside a beam of 40 MHz with bunch spacings of 25 ns, and a small beam size at the interaction points enable a high luminosity. The instantaneous luminosity is a key parameter for the collider, describing the number of collisions per unit area per second at an interaction point in $\mathrm{cm^{-2}\,s^{-1}}$ [4]. Whereas the total number of potential collisions per unit area for a given period of time is called the integrated luminosity. The collisions take place in four experiments:

- ATLAS (A Torodial LHC Apparatus), a general-purpose detector,
- CMS (Compact Muon Solenoid) detector, a general-purpose detector,
- LHCb (Large Hadron Collider beauty), specialized on quark flavors,
- ALICE (A Large Ion Collider Experiment), specialized on heavy ion collisions.

The LHC started operating in 2009; the first data-taking phase from 2010-2012 is referred to as Run 1 and reached a center-of-mass energy of $\sqrt{s} = 7\,\mathrm{TeV}$. The center-of-mass energy was raised to 8 TeV in 2012. After that, the Long Shutdown 1 followed, for maintaining purposes and upgrading the detectors and the accelerator. Run 2 from 2015-2018 achieved a center-of-mass energy of $\sqrt{s} = 13\,\mathrm{TeV}$ and the currently proceeding Run 3, started in 2022, almost reaches the LHCs design energy of 14 TeV with a center-of-mass energy of 13.6 TeV [6]. Also the proton-proton collision rate was elevated from an instantaneous luminosity of $7.7 \times 10\,\mathrm{cm^{-2}\,s^{-1}}$, at the end of Run 1 [3], to $2 \times 10^{34}\,\mathrm{cm^{-2}\,s^{-1}}$ in Run 2, exceeding its design value of $1 \times 10^{34}\,\mathrm{cm^{-2}\,s^{-1}}$ [4].
Current research area is the expansion of the Standard Model of particle physics, to be able to explain for instance the lack of anti-matter in our universe and the constituents of dark matter [4].
For further investigation, the LHC will go into the Long Shutdown 3 in December 2025 until the upgrade of the LHC to the High Luminosity LHC (HL-LHC) is completed. The HL-LHC is foreseen to operate until 2041 [7], and to achieve an instantaneous luminosity of 5 - 7.5 $\times$ $10^{34}\,\mathrm{cm^{-2}\,s^{-1}}$[3].

2.2. The CMS (Compact Muon Solenoid) experiment

The CMS detector is composed of many subdetectors, which are arranged cylindrical in barrel form in the central part enclosing the interaction point, and in so-called discs at the endcaps, orthogonal to the particle beam. The most-inner subdetectors are the tracking detectors, consisting of a silicon pixel and a silicon strip detector, to measure the trajectories of charged particles. The tracker is enclosed by the electromagnetic and the hadron calorimeters (ECAL and HCAL), which measure the energy of primarily electrons and photons, and hadrons, respectively. These calorimeters absorb the entire energy of these particles, allowing for precise energy measurements. Further outside follows the eponymous superconducting solenoid magnet, which generates a magnetic field of 3.8 T. The Lorentz force bends the trajectories of charged particles passing through it. By measuring the bending angle, the transverse momentum of the particles relative to the beam pipe can be determined. The most outer layer is formed by a muon chamber system, which measures the trajectories and transverse momenta of muons, permeated with the heavy iron return yoke.
Together with the mechanical support structures, readout electronics, and cooling supply lines, they form a 29 m long detector with a diameter of 15 m, weighting 14000 t, which can be seen in Fig. 2.1. The present detector covers the pseudorapidity[1] up to $|\eta| = 2.4$.

[1]The CMS coordinate system places the origin at the collision point within the detector, with the y-axis pointing upward and the x-axis radially inward toward the LHC center. The z-axis aligns with the beam direction. The azimuthal angle ϕ is measured from the x-axis in the x-y plane, with the radial coordinate r. The polar angle θ is measured from the z-axis. The pseudorapidity η is defined as $-\ln \tan(\theta/2)$ [9].

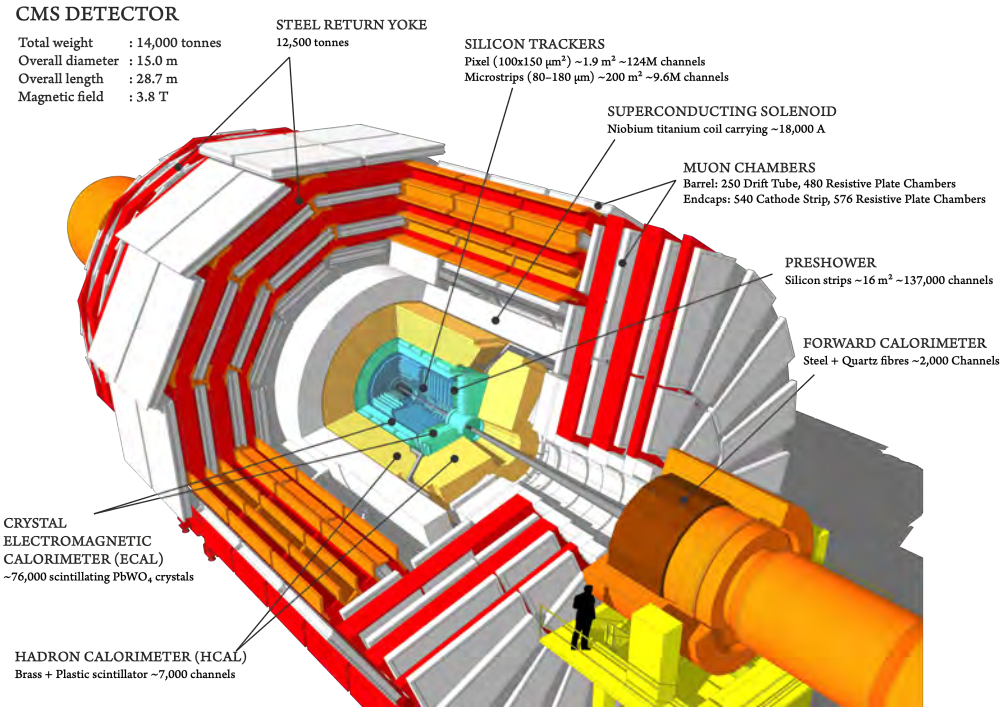

Figure 2.1: A 3D model of the CMS detector shown in a cutaway view. The small notes explain the subdetectors [8].

A relevant part is also the trigger system, which selects interesting collision events to reduce the event rate of 40 MHz. Given that a new bunch crossing occurs every 25 ns, with approximately 50 collisions on average in Run 3 [10], the amount of data is too large to be stored and processed in its entirety. The trigger consists of two stages: the Level-1 (L1) trigger and the High-Level Trigger (HLT). The L1 trigger is hardware-based and reduces the rate of events with an output limit of 100 kHz, based on coarse information from the calorimeters and muon system. Accepted events then undergo further evaluation in the software-based High-Level Trigger. The HLT uses the complete read-out detector data of the event for complex offline analysis, further reducing the output rate of events to 1 kHz. The time it takes for the trigger to make a decision is called latency. The L1 trigger latency is approximately 3.2 µs [4, 9].
During Run 3, an integrated luminosity of 73 fb^{-1} has been recorded so far by CMS, with the goal to reach 300 fb^{-1} at the end of the run time [10].

2.3. The High Luminosity LHC

The LHC will enter into the Long Shutdown 3 in 2025, to elevate the luminosity and to extend the lifetime of the LHC, by being upgraded into the new High Luminosity LHC (HL-LHC).
The integrated luminosity is expected to increase by an order of magnitude, resulting in an expected collection of an integrated luminosity of 3000 fb^{-1} of data during the HL-LHCs lifetime in the nominal scenario, with a potential of reaching up to 4000 fb^{-1} in an ultimate scenario. The focusing properties of the beam significantly influence the transverse beam size, which is called β^*. A smaller beam size will be obtained with new wide aperture inner triplet magnets and together with a higher bunch population will result in the desired luminosity increase.
The upgrade will yield a higher pileup, and therefore a higher hit rate with 140 - 200 simultaneous interactions per collision. This demands for an improvement of the trigger, the readout electronics and a higher granularity of the subdetectors, to handle the increased particle and track density. Also the radiation levels and potential radiation damage are expected to rise by an order of magnitude. The upgraded subdetectors must withstand high radiation levels while providing reliable data throughout their operational lifespan. A challenge are the inner subdetectors, such as the tracker, since they are inaccessible once built in, and are closest to the collision point. They have to stand the highest radiation levels. The present tracker will be entirely replaced with a new pixel and strip tracking detector, which is also designed to provide information to the Level-1 trigger, enabling an even more effective selection of relevant events in higher pileup environment. The L1 trigger rate will increase from 100 kHz to 750 kHz, with latency increasing from 3.2 µs to 12.5 µs. Also the muon and calorimeter systems will provide information to the L1 trigger. The calorimeters will get new endcaps, which combine the functions of the ECAL and HCAL, using silicon sensors and scintillating tiles as active elements. Except for upgraded electronics, the muon chambers do not require replacement; however, new chambers will be added in the forward region. Additionally, a completely new timing detector will be installed, which will help to distinguish the particles by measuring the arrival time of the particles from the up to 200 simultaneous collisions with a precision of 30 - 50 ps [4].

2.3.1. The CMS Phase-2 tracker upgrade

For the CMS Phase-2 upgrade, the whole tracker will be replaced. The new tracker will be divided into the Inner Tracker (IT), using silicon pixel modules as detecting devices, and the Outer Tracker (OT), which utilizes so-called PS modules, consisting of a silicon strip and a macro-pixel sensors, and 2S modules, consisting of two strip sensors. The Outer Tracker is divided in a barrel part, located close to to the interaction point, and endcaps on both sides. The barrel region of the OT comprises six layers, divided into the tracker barrel with PS modules (TBPS) for the first three layers and the tracker barrel with 2S modules (TB2S) for the outer three layers. The endcaps are structured as discs, consisting of five endcap double-discs, referred to as the Tracker Endcap Double-Discs TEDD [3]. The endcaps are further subdivided into TEDD 1 and TEDD 2, distinguished by their radii to host the IT support tube. The whole tracker layout can be seen in Fig. 2.2. The discs are formed with light-weight carbon fiber support structures equipped with PS modules in the inner part with a radial distance below 60 cm [4], and 2S modules in the outer part. A disc is formed by combining two D-shaped part, the so-called dees [3]. One dee consists of two carbon fiber skins, with a cooling pipe embedded. Inserts are protruding out of the surface and provide the cooling connection to the modules. The aluminum inserts have a cylindrical shape and employ a cooling surface with a diameter of 8 mm. They are glued to the CO_2 pipe, made of stainless steel. The inner diameter of the pipe will be either 2.20 mm or 2.40 mm, depending on the position in the endcap [11]. Overall, there will be six different insert types, which mainly vary in their length. Each dee contains seven cooling circuits. The remaining space between the surfaces is filled with the light polyetherimide foam 'Airex'. Tracking modules are positioned on both the front and back sides of the dees, ensuring full hermiticity with four module layers in a fully assembled double disc, consisting of two discs staggered along the beam pipe axis. A CAD drawing of a fully populated TEDD can be found in the left Fig. 2.3. The new tracker will extend its range of pseudorapidity up to $|\eta| = 4$ [4].

The design of the Outer Tracker is mainly driven by the requirement to provide information to the L1 trigger. This is achieved by employing modules equipped with two silicon sensors stacked on top of each other, which measure the trajec-

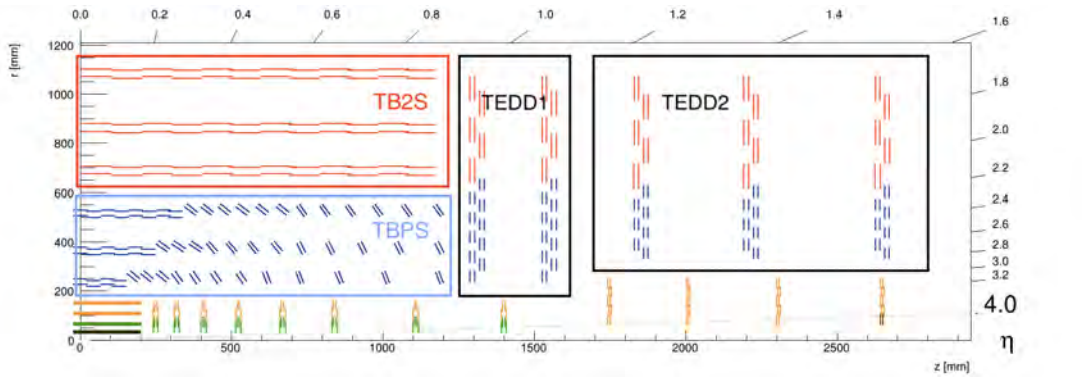

Figure 2.2: Layout of one quarter of the Phase-2 tracker. The pixel modules of the Inner Tracker are depicted in yellow and green. Further outside is the Outer Tracker, with PS modules shown in blue and the 2S modules in red. Modified from Ref. [3].

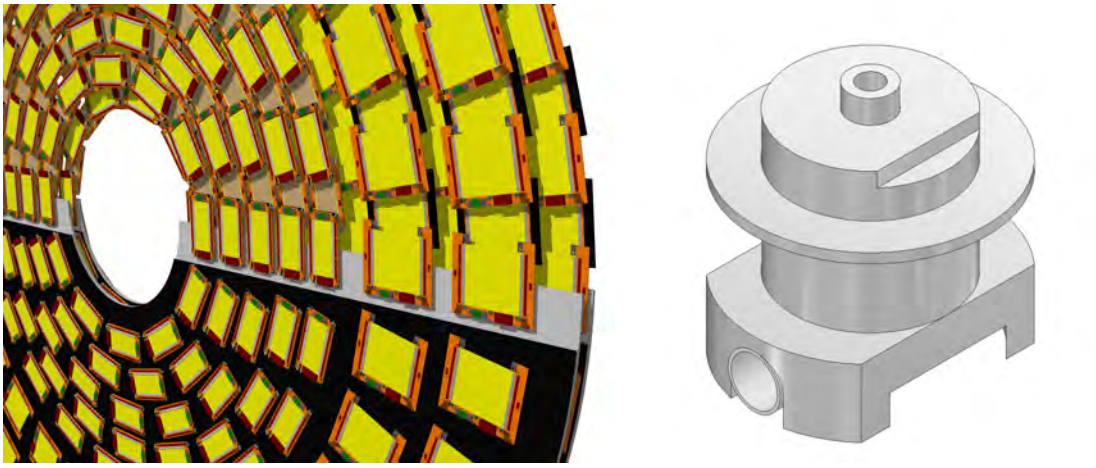

Figure 2.3: Left: a CAD drawing of a TEDD structure with mounted p_T-modules [3]. Right: a CAD drawing of an insert [11, 12].

tories of the particles and identify those with a high transverse momentum p_T. The new modules are designed to compare the hit patterns of the two sensors for correlating hit pairs, which are called stubs. Consequently, the 2S module can estimate the p_T of particles, identify those with a transverse momentum that exceeds a programmable threshold, and provide this information to the L1 trigger [4, 3].
To reconstruct the p_T value in every tracker region, different sensor spacing values are used for the silicon modules [3].
To improve granularity, the silicon sensors are made very small, with pixel dimensions in the tens of microns for 3D measurements, and the silicon strip sensor length in the dimensions of a few centimeters for 2D measurements. The pixel modules are only used in proximity to the collision point – the region with the highest hit density. Further away, the decreasing granularity is sufficient, saving a lot of cost and reducing the required readout bandwidth [4].
In regards of radiation hardness, it is known that the irradiation causes an increase of depletion voltage and leakage current in the sensors [3], by damaging the silicon crystal lattice. As the leakage current is exponentially dependent on the sensor temperature, the module can be at risk to enter in a thermal runaway, where it experiences a self heating loop, if the cooling power is not sufficient. A new evaporative CO_2 cooling system is used at Phase-2, which achieves cooler temperatures than the present one based on liquid C_6F_{14} and therefore also reduces the noise[4].
The new cooling system is based on the 2-Phase Accumulator Controlled Loop (2PACL) concept [3]. It evaporates one part of the CO_2 while another part remains in its liquid state. As the received heat load is used as latent heat for a phase change from the liquid phase to the gaseous phase, the cooling temperature is almost not affected and thereby almost independent on the heat load. The vapor pressure is dependent on the CO_2 temperature. The new system can achieve a temperature down to $-35\,^{\circ}\mathrm{C}$, unlike the present mono-phase refrigerant C_6F_{14}, which runs at a temperature of about $-20\,^{\circ}\mathrm{C}$, but will range up to $-33\,^{\circ}\mathrm{C}$ along a cooling circuit in the TEDD. The new cooling system can run at lower temperatures, can be run with smaller pipe diameters, and is cheaper and more environmentally friendly than the present cooling system [3, 4].

3. The 2S module

3.1. Design of the 2S module

The 2S module consists of two n-in-p doped silicon strip sensors that are closely stacked on top of each other.
The sensors employ multiple 5 cm-long strips with a pitch of 90 µm. Two rows of silicon strips form a $10 \times 10\,\mathrm{cm}^2$ sensor area with an active thickness of 290 µm. One silicon sensor has 1016 strips; one 2S module has therefore a total of 4064 channels [13]. The strips are reverse-biased with a "bias voltage" of $-300\,\mathrm{V}$ for unirradiated sensors and $-600\,\mathrm{V}$ up to $-800\,\mathrm{V}$ for irradiated sensors in the detector. The sensors are glued to spacers, so-called bridges, made of an aluminum/-carbon fiber composite (AlCF). The front-end hybrids (FEH) are glued to two long spacers positioned on opposite sites, while the service hybrid, connecting the two FEHs, is glued to a short spacer, called stump bridge. The spacers provide mechanical support and maintain a gap between the two silicon sensors. The 2S modules are built with the two sensor gap widths 1.8 mm and 4 mm. The spacers have a high thermal conductivity and provide the contact points for the 2S module to be screwed onto the inserts to remove the heat from the silicon sensors and from the read-out electronics. Certain 2S modules, such as those populating the TEDD, possess an additional sixth cooling contact on the opposite side of the service hybrid [3].
The silicon sensors are wire-bonded to the front-end hybrids (FEH) on both the left and right sides. The 2S module can be seen in the CAD drawing in Fig. 3.1.
Always the left side of the top and bottom sensor, and the right side of the top and bottom sensor are read out on their respective sides. Each front-end hybrid carries eight CMS Binary Chips (CBC) for read-out and one Concentrator Integrated Circuit (CIC), serving as an interface between the CBCs and the readout link. It has the purpose to aggregate and serialize the data. The FEHs are laminated onto stiffeners, which are Carbon Fiber Reinforced Polymer supports (CFRP). As the FEHs read out both the top and bottom sensors, the circuits are folded around

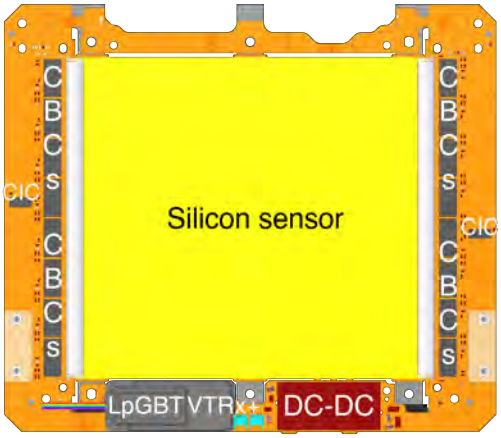

Figure 3.1: A CAD drawing of the 2S module with labelled components [12].

the spacers and wire-bonded [3].
The service hybrid hosts the components for a back end connection, which is provided by three wires and two optical fibers [4]. The LpGBT chip (de-)serializes the data from (to) the back end. The VTRx+ is an optoelectric transceiver and converts the data to optical (electrical) signals [3]. The DC-DC converters step down the input voltage of up to 12 V in two stages to 2.55 V and 1.25 V, supplying the power for the module electronics [3, 4].
The three hybrids collectively generate approximately 5.2 W of power. The power consumption of the eight CBCs and the CIC amounts to approximately 1.3 W per FEH. The service hybrid has a power consumption of about 2.6 W, dominated by the heat dissipation from the DC-DC converters, estimated to be around 2 W due to efficiency losses. The power generated by the silicon sensors is determined by the leakage current multiplied by the bias current. In the nominal scenario, this power consumption is estimated to 0.47 W per sensor.
This yields a total module power of about 6.1 W for a 2S module in the nominal scenario [11].

3.2. Thermal runaway

The modules will be inaccessible, once installed. Therefore it is important to guarantee that they can provide valuable measurement data during their whole lifetime. Since the tracker is closest to the beam and collision point, it is exposed to the strongest radiation level. The radiation fluence Φ is stated in 1 MeV neutron equivalent per 1 cm^2, n_{eq}/cm^2. The fluence in the location with the worst cooling conditions in the TEDD is in TEDD 2 on ring 11 of disk 3 with $3.73 \times 10^{14}\, n_{eq}/cm^2$ for a nominal operation scenario [14].
Irradiation damages the silicon crystal lattice of the sensors over time and therefore increases the needed bias voltage and the leakage current. Since the sensor current is exponentially dependent on the sensor temperature, large leakage currents can induce overheating. It enters a self heating loop, so-called thermal runaway, which can leave the module inoperable, if the cooling capacity is not sufficient [3, 4].
The dependency of the leakage current on the sensor temperature is given by the following Equation 1 [15]:

$$I_{Leakage}(T_{Sensor}) = \alpha \cdot A_{Sensor} \cdot d_{active} \cdot \Phi \cdot \left(\frac{T_{Sensor}}{T_0}\right)^2 \cdot exp\left(-\frac{\Delta E}{2k_B}\left(\frac{1}{T_{Sensor}} - \frac{1}{T_0}\right)\right). \quad (1)$$

The variables include the leakage current $I_{Leakage}$, the damage constant α, the sensor area $A_{sensor} = 2{\times}10{\times}10\,cm^2$, the thickness of the active material $d_{active} = 290\,\mu m$, the fluence Φ, the sensor temperature T_{Sensor}, the reference temperature $T_0 = 20\,°C$, and the Boltzmann constant k_B. The energy $\Delta E = 1.21\,eV$ refers to the band gap of silicon at the reference temperature T_0.

Three radiation and operation scenarios for the HL-LHC are considered by CMS, the nominal scenario after 3000 fb^{-1}, and the so-called Ultimate@600V and Ultimate@800V scenario after 4000 fb^{-1}. They describe different values for the expended fluence on the module, which is dependent on the location in the detector,

and different values for the bias voltage of the silicon sensors, and the radiation damage constant for silicon. The power equation Eq. 1 is dependent on these values, which are displayed in Tab. 1.

Scenario	Bias voltage in V	α in A/cm	Φ in n_{eq}/cm^2
Nominal	600	$4.28 \cdot 10^{-17}$	$3.73 \cdot 10^{14}$
Ultimate@600V	600	$4.28 \cdot 10^{-17}$	$4.96 \cdot 10^{14}$
Ultimate@800V	800	$5.14 \cdot 10^{-17}$	$4.96 \cdot 10^{14}$

Table 1: Parameters of the bias voltage, the radiation damage constant α, and fluence Φ for the three considered scenarios at the HL-LHC for the specific module location [14, 16]

In this thesis, the thermal runaway is investigated in the Ultimate@800V scenario. It assumes a rise in fluence of 33 % to 4.96×10^{14} and a raise in the bias voltage of 33 % to 800 V, compared to the nominal scenario [3, 16]. The induced increase in leakage current results in an increase in sensor power, leading to a rise in sensor temperature. The minimum CO_2 temperature at which the cooling power is insufficient and the thermal runaway occurs is important to know. Already realized simulations predict a margin of 9 K between the nominal CO_2 temperature of $-33\,°C$ and the start of the thermal runaway in the nominal scenario [3].
This margin will be investigated for the Ultimate@800V scenario in this thesis.

4. Setup

For this thesis, thermal measurements have been performed with a 2S module and heating resistors, mounted on a small mock-up of a TEDD disk built by the CMS working group at DESY [17] and further referred to as mini-TEDD structure. For heat flux investigations, the mini-TEDD has to be equipped with temperature sensors on the top and bottom side. It is cooled by two-phase CO_2, simulating the expected conditions in the detector on a small scale. For the usage of two-phase CO_2 at comparable conditions as expected in the detector, a custom CO_2 cooling system unit was developed, constructed, and operated by the CMS working group of the Physics Institute 1B at RWTH Aachen University [18]. The cooling system is directly connected to the mini-TEDD. To minimize heat exchange between the active 2S module and the ambient air, the unit is placed in a cooling box, which is connected to an external chiller, to match the ambient temperature with the mean module sensor temperature. The mini-TEDD structure inside the cooling box can be seen in Fig. 4.1. The module cooling box itself has been developed by Max Rauch as part of his PhD thesis at the Physics Institute 1B [19] and was constructed by the CMS working group at Aachen.

To simulate an irradiated 2S module, LED strips are used to generate leakage current in the silicon sensors. To produce equal power load on the top and bottom sensor, LED strips are mounted on the mini-TEDD structure and the cover of the cooling box; the generated current is controlled and adjusted with a PID control.

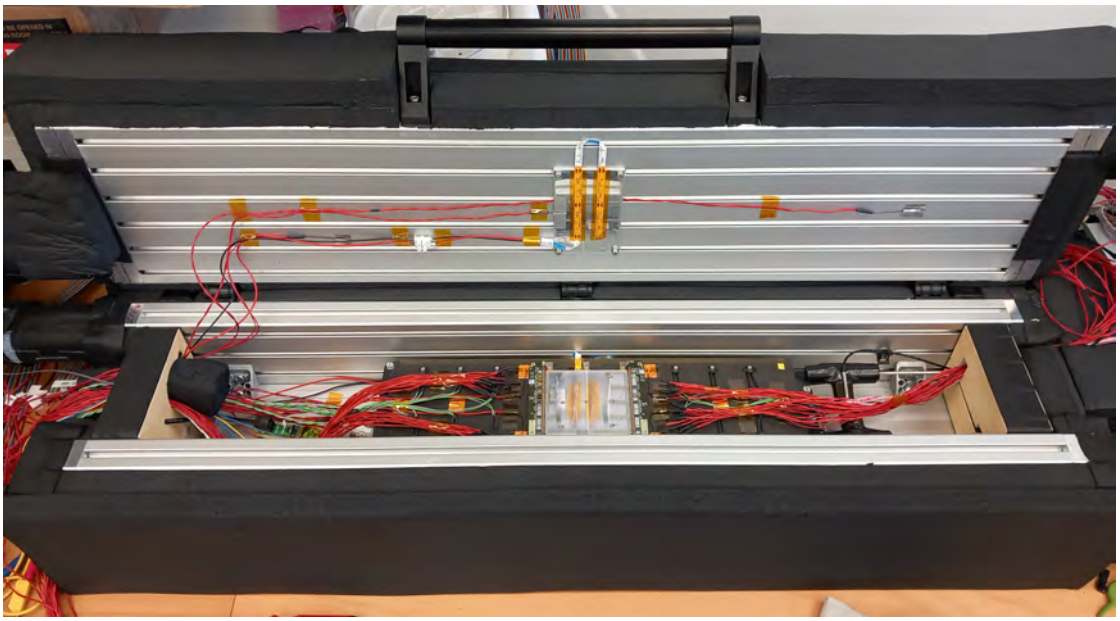

Figure 4.1: Cooling box with the 2S module on the mini-TEDD structure placed inside at the height of the CO_2 pipes to the right. The cooling box is flushed with dry air and cooled by an external chiller. The red wires of the thermistors are guided outside of the compartment through both the left and right feedthroughs.

4.1. Mini-TEDD structure

The mini-TEDD consists of a cooling pipe, composed of stainless steel and carrying the CO_2 in a U-turn shape. Aluminum inserts are affixed along the pipe and protrude from the carbon fiber surface to function as both cooling contacts and mounting points for the module. On the mini-TEDD, the two insert types, short and long, are used; in this set-up the long inserts are turned facing upwards and the short inserts face downward. The outer pipe diameter of 2.2 mm and the inner pipe diameter of 2.0 mm, as well as the insert dimensions are consistent with the final dee dimensions in TEDD 1 [3].
There are three possible module positions on top and three on the bottom side of the mini-TEDD structure, so it can host up to six possible modules in total. One position always includes six cooling contacts. Since the inserts are sequenced along the pipe, the top and bottom module positions alternate accordingly. A picture of the mini-TEDD structure can be seen in Fig. 4.2.
In Figure 4.3, a CAD drawing of a cross section of the mini-TEDD middle position [12] can be seen, showing one pipe in the middle position. The pipe is enclosed by two carbon fiber skins with inserts protruding up and downwards. The short insert has a main yellow part, composed of aluminum and a red part, called an insert support, composed of plastic material [3]. The long insert next to it has a yellow and pink part, both composed of aluminum. The main part is the yellow one, but the pink part protrudes from the carbon fiber skin too.

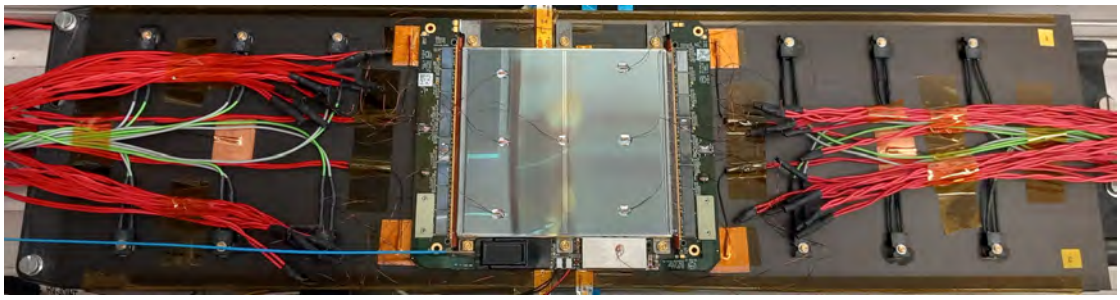

Figure 4.2: Picture of the cooling structure with heating resistors and 2S module mounted on top. The visible top side can host up to three 2S modules with six cooling contacts and employs long inserts. The non-visible bottom side can also host up to three 2S modules and employs short inserts.

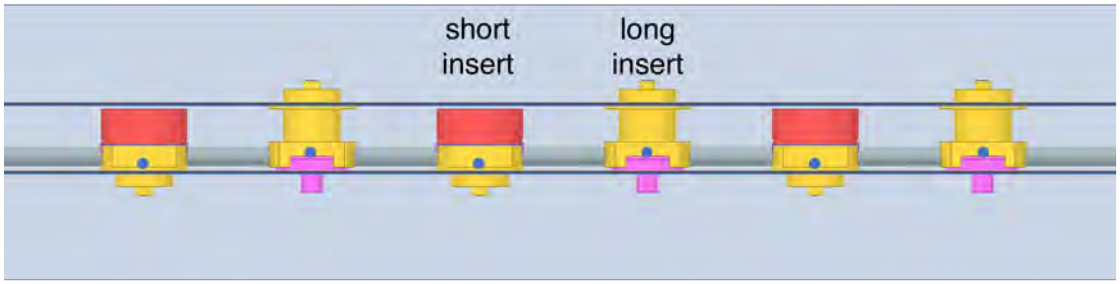

Figure 4.3: CAD drawing of a cross section of the mini-TEDD middle position. The short and long inserts protrude from the carbon fiber skins and are affixed to the CO_2 pipe. The blue dots indicate the location of temperature sensors [12, 11].

The blue dots indicate the locations of NTC temperature sensors, which are glued onto the inserts of the middle position.
Between the carbon fiber skin, the pipe is embedded in Airex foam. To be able to measure temperatures directly at the inserts, 15 temperature sensors are glued to the pipe and the inserts of the middle module positions. Channels, housing the wires, are cut into the foam as seen in Fig. 4.4 [20].
The temperature sensors inside the mini-TEDD are labeled as shown in Fig. 4.5. Thermistors are also placed on top of the CO_2 pipe, position 1 at the inlet, position 2 at the U-turn and position 3 at the outlet. The temperature sensors are read out by a Keithley Multimeter 2701 [21].

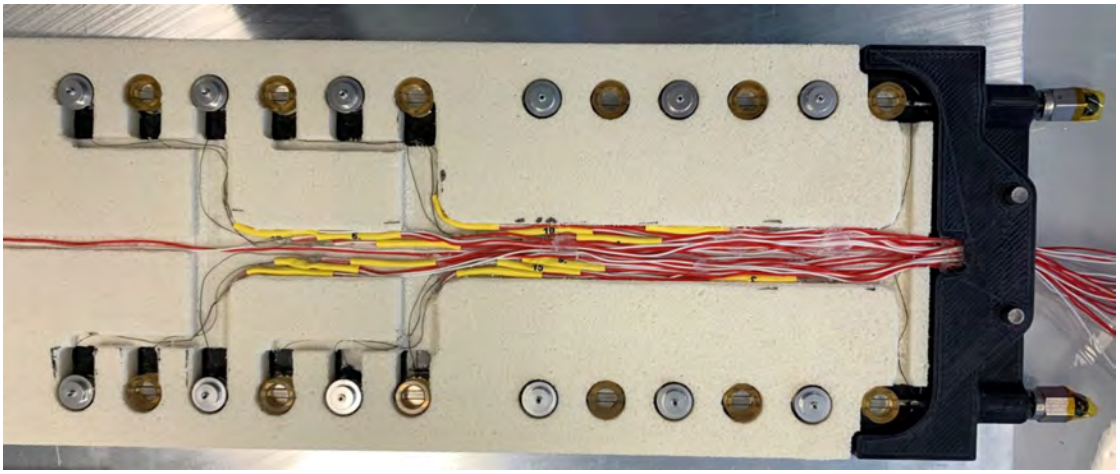

Figure 4.4: The Mini-TEDD structure during construction without the upper carbon fiber skin. It is filled with Airex foam with channels carved into the foam to house the wires of the temperature sensors on the inserts of the middle position and on the pipe [20].

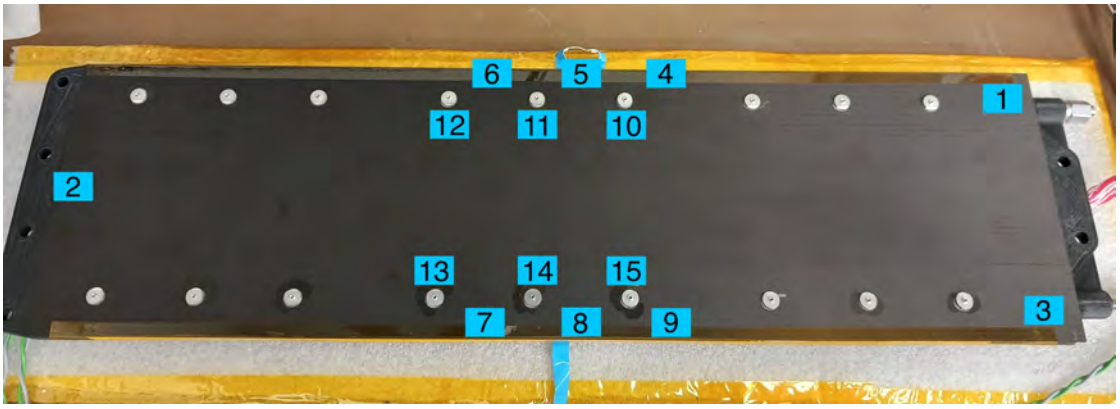

Figure 4.5: Mini-TEDD structure shown from above. The numbers 10 - 15 label the temperature sensors glued to the visible long inserts, while the numbers 4 - 9 label the thermistors on the short inserts on the bottom side. The numbers 1, 2 and 3 label thermistors glued on top of the CO_2 pipe, 1 at the CO_2 Inlet, 3 at the Outlet and 2 at the U-turn of the pipe.

4.2. Thermistors and heating resistors

For the thermal measurements of this thesis the 2S module 2S_40_6_AAC-00003 with six cooling contacts and a sensor spacing of 4.0 mm has been used. The silicon sensors of the 2S module are supplied with high voltage by a Keithley 2410 SourceMeter [22] and the low voltage is supplied by a Hameg HMP 4040 [23]. The module has been equipped with multiple temperature sensors by Vanessa Oppenländer in the framework of her master thesis at the Physics Institute 1B [11]. To determine the mean sensor temperature of the silicon sensors, seven thermistors are glued onto the top and bottom sensor, respectively. Additionally, further thermistors are glued onto the hybrids to survey the heat distribution, particularly on the CIC, CBC, VTRx+, LpGBT and the spacers. The module has been mounted on the middle position of the mini-TEDD and screwed onto the six long inserts with a washer and M1.6 screws made out of brass with a torque of 10 cNm, which has been found to be the optimal torque, to improve the thermal contact [11].

4.2.1. Gluing of temperature sensors onto the carbon fiber surface

To gain an understanding of the heat flow of the module and the cooling structure, small NTC temperature sensors [24] are mounted on the top and bottom side using copper tape. Four sensors are mounted in the center of the right and left module position on both the top and bottom side. On the top side next to the module (ntm), four thermistors are placed along the pathway of the CO_2 pipe, both on the left and right side of the module. On the bottom side, four thermistors are placed between the short inserts (bi) and the backside of the long inserts. For simple comparison, the new directions "north" and "south" are introduced: looking down at the top of the unit, the CO_2 inlet refers to north, while the CO_2 outlet refers to south. The exact locations and names are visualized in Fig. 4.6.

The mounted module with thermistors glued onto it can be seen in Fig. 4.2. Due to the limited number of channels of the Keithley, not all available sensors can be read out, for example the temperature sensor on the DC-DC is not read.

4.2.2. Mounting of heating resistors on remaining module positions

To simulate a full population of the mini-TEDD, heating resistors are placed on the five remaining positions. With the 2S module placed on the top side in the middle position, for each of the other five positions on the top and bottom side six heating resistors resembling one module are screwed on the inserts. The heating resistors each have a resistance of 200 Ω and are screwed onto the inserts with a torque of 8 cNm. During the thermal measurements, the resistors are operated to emulate a 2S module with a nominal power of 6 W, supplied by a second Hameg HMG 4040. Therefore the voltage draw for the parallel wired heating resistors is 14.14 V, resulting in approximately 1 W of power load put into each insert by a single heating resistors. The voltage drop on the wires is insignificant. The whole carbon fiber structure with mounted heating resistors and thermistors with and without the 2S module can be seen in Fig. 4.7.

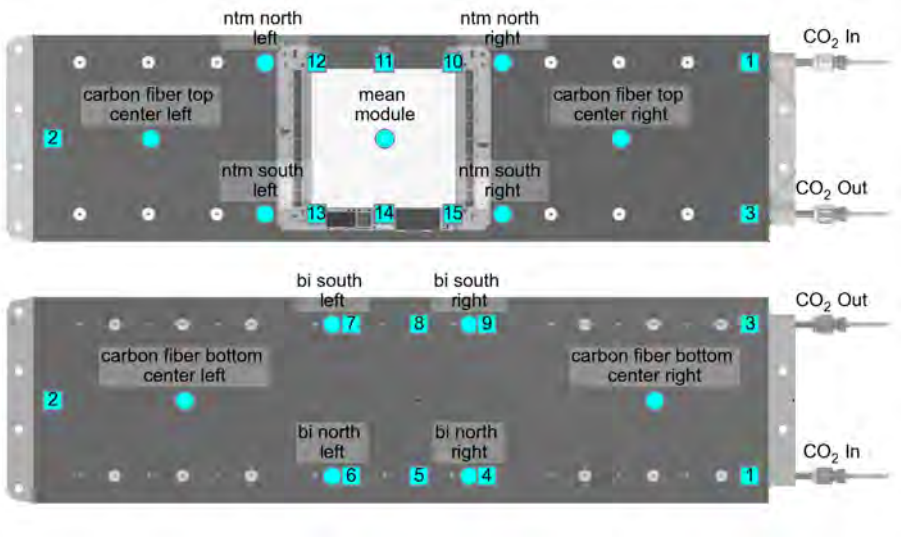

Figure 4.6: The carbon fiber structure pictured with exact locations and labels of the thermistor positions in blue. The upper depiction shows the top side of the mini-TEDD structure with the mounted 2S module. The depiction below shows the bottom side. The squares refer to the numbering of the thermistors inside the mini-TEDD at the inserts, while the dots refer to the locations of the thermistors on the cooling structure itself. On the top side, the thermistors are placed next to the module (ntm) while the bottom thermistors are placed between the inserts (bi). In the center of the left and right module positions, thermistors are placed both on the top and bottom side.

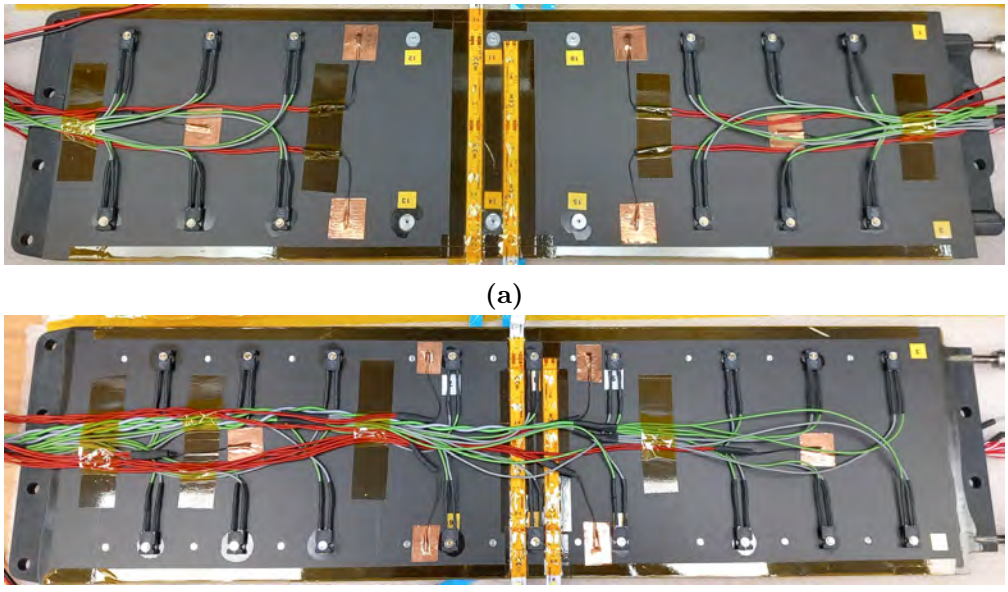

(a)

(b)

Figure 4.7: (a) Photo of the cooling structure with heating resistors. The heating resistors employ green wires, while the thermistors employ red wires and are fixed in position with copper tape. A LED strip is mounted centrally under the 2S module. Photo (b) shows the bottom side. Three heating resistor 'modules' are mounted on the module positions with short inserts. The thermistors are fixed between the long and short inserts (bi). The LED strip is not used.

4.3. Module cooling box and CO_2 cooling system

The module cooling box in Fig. 4.1 was built using ITEM profiles and is insulated by two 3 cm thick Armaflex layers. An external chiller is connected at the left of the box and uses the hollow lateral cross sections of the ITEM profiles to carry the coolant. For the thermal measurements the chiller HUBER CC 505 [25] was used with silicon oil M60 as coolant. It can achieve temperatures down to $-42\,°C$, with the inner box temperature usually being 1 - 2 K warmer. Insulating blocks are placed to the left and right of the inner box volume, provided with feedthroughs for both CO_2 pipes and the wires of the electronics to guide them outside. The grooves on the bottom of the box are covered with caps. The resulting space between the grooves and the caps is flushed with dry air, cooling it before entering the inner volume through small vents in the caps. During the thermal measurements, the air flow is regulated with a flow meter to 4 l/min. A low humidity level inside the box is necessary to prevent condensation on the module and pipes during cooling. The humidity is measured with a LabKit hygrometer [26] placed to the left of the mini-TEDD. The measured humidity is used to calculate the dew point, which should always be below the 2S module sensor temperature. Thermistors are fixed to the walls of the box under the module on the left of the module, and on the cover with aluminum tape to measure the ambient and box temperature. A LED strip is placed on a movable aluminum plate on the cover above the module and on the cooling structure beneath the module, to induce adjustable current in the silicon sensors to simulate radiation damage in the unirradiated module.

The CO_2 cooling system is based on the 2PACL method and controls the CO_2 temperature along the vapor pressure curve. In the Appendix in Fig. A.2, a photo of the CO_2 cooling system can be found. In the system, an expansion vessel [27] is used as an accumulator vessel. Subsequently, the CO_2 passes through an actively cooled heat exchanger, the CO_2 pump [28], a passive heat exchanger, and a preheating loop before entering the module cooling box. Both the expansion vessel and the actively cooled heat exchanger are connected to a Huber unistat 815 cooling unit [29], respectively. The pump operates at a rotational frequency of 2600 rpm during the thermal measurements. The preheating loop is connected to a power supply operating at 10 W, and applies a small heat load to the CO_2 cooling pipe before entering the box. A flow meter is installed in the cooling circuit too, but was broken during all measurements in this thesis. The expected CO_2 mass flow is 1.6 g/s in the TEDD 2 region, which was achieved with the rotational frequency of 2600 rpm in previous measurements [11]. To be comparable, this frequency was also applied for these measurement. Multiple temperature sensors are mounted along the cooling circuit, and additional sensors measure the pressure between the expansion vessel and the actively cooled heat exchanger, as well as before the preheating loop. A schematic overview can be found in the Appendix in Fig. A.1. The devices are controlled and read out via a LabView program [30], providing a graphical user interface to monitor the temperature profile during a thermal measurement.

4.3.1. Determination of the CO_2 temperature in a comparison of methods

The purpose of the thermal runaway measurements is to determine the CO_2 temperature at which the onset of thermal runaway occurs. Therefore it is crucial to ensure reliable and accurate measurements of the CO_2 temperature.
To achieve this, new PT100 temperature sensors have been installed at the inlet and outlet of the mini-TEDD. The PT100 temperature sensors are positioned at the pipe connections to the mini-TEDD structure. Therefore, t-pieces are affixed between the mini-TEDD and the CO_2 pipe, with the PT100 sensors tightly inserted into the t-pieces. The sensors are inserted just until they barely meet the pipe opening to keep the influence on the flux at a minimum. The PT100 sensors have a resistance of $100\,\Omega$ at $0\,°C$ and are read out using a four-point measurement [31]. A picture of sensors can be found in the Appendix, depicted in Fig. A.3.

To validate the accuracy of the PT100 temperature sensors, their measurements can be compared to the measurements of the sensors on top of the pipe inside the mini-TEDD and the temperature that results from the pressure measurements. In Figure 4.8, the left plot shows a exemplary CO_2 temperature measurement for the PT100 sensors and the thermistors on the pipe within the cooling structure, while the right plot shows a comparison of the CO_2 temperatures at different silicon sensor temperatures, taken during thermal runaway measurements with only the

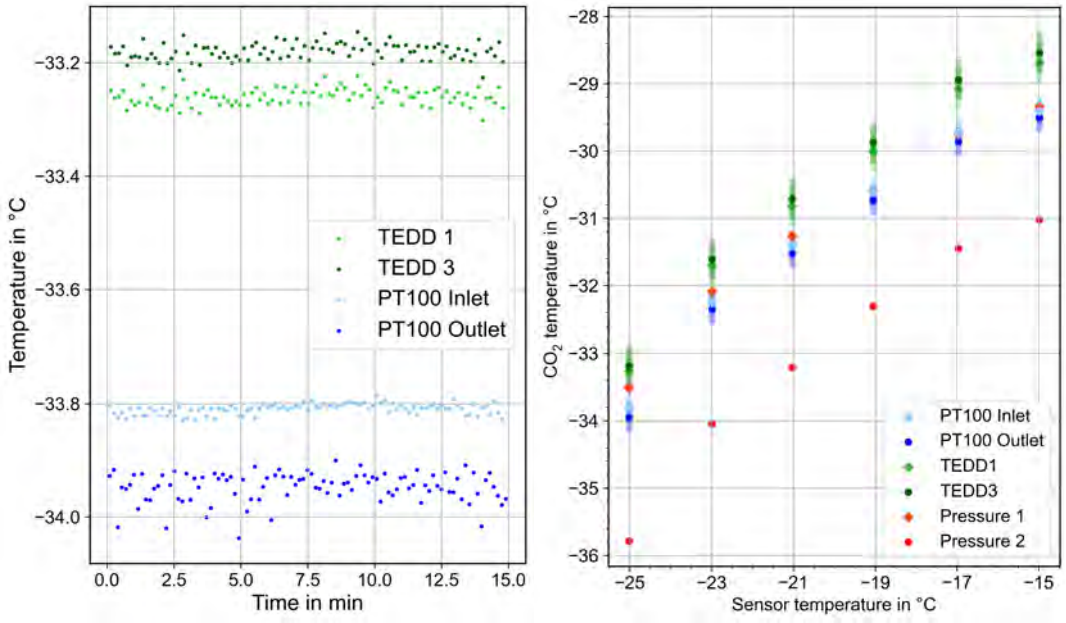

Figure 4.8: Left: the CO_2 temperature profile for the PT100 sensors and the thermistors inside the mini-TEDD during measurement of the data point at a CO_2 temperature of $-33.9\,°C$, a silicon sensor temperature of $-25\,°C$, and equal ambient temperature for 15 minutes. Right: CO_2 temperatures of the PT100 sensors, on the pipes within the mini-TEDD structure, and the temperature calculated from the pressure for different silicon sensor temperatures. The displayed temperatures were taken during the thermal runaway measurement with the 2S module alone powered. The semitransparent bars indicate the systematic uncertainties.

2S module activated.
The measurement depicted in the left plot of Fig. 4.8 was conducted at a CO_2 temperature of $-33.9\,°C$ and a silicon sensor temperature of $-25\,°C$ for a duration of 15 minutes. It can be observed that the temperature deviation of the TEDD sensor is approximately the same for the inlet and outlet. The highest standard deviation for the TEDD sensors across all measurements is 0.018 K. Their systematic uncertainties are 0.3 K, as determined by Vanessa Oppenländer in Ref. [11]. The PT100 outlet temperature exhibits a wider spread compared to the inlet temperature, for reasons currently unknown. The highest standard deviation for the PT100 outlet across all measurements is 0.09 K, whereas for the inlet, it is 0.012 K. The systematic uncertainty for the PT100 sensors has been calculated individually for each measurement point, with the highest uncertainty being 0.22 K. This calculation has been performed using Eq. 2, displayed in the Appendix.
In the right plot of Fig. 4.8 it can be seen that the PT100 inlet and outlet temperatures only differ by about 0.2 K for the most part. As expected, the outlet is cooler than the inlet. The CO_2 removes the heat load of the insert caused by the active module. Liquid CO_2 evaporates during the removal, causing the pressure to decrease and the temperature to drop. The measured temperatures of the mini-TEDD are warmer by about 0.7 K, as expected since they are installed at the outside of the pipe. At the mini-TEDD inlet and outlet, 1 is located at the inlet and is also supposed to be slightly warmer than 3, located at the outlet. But since the difference is only miniscule with about 0.1 K, this discrepancy remains within the tolerance of the systematic uncertainties, which has been found to be 0.3 K [11]. The measured pressures can be used to calculate the CO_2 temperature along the vapor pressure curve, and for that purpose, a CO_2 calculator [32] has been used. Pressure 1 is measured before entering the preheating loop. Therefore it is expected to be warmer than the inlet, since the heat load, received inside the loop, causes the CO_2 temperature to drop slightly. Pressure 2 is taken between the expansion vessel and the active heat exchanger. This pressure measurement is expected to have a lower pressure, and consequently a lower temperature, than Pressure 1, due to the pressure decrease along the cooling circuit. In conclusion, the measured temperature behavior is as expected and the CO_2 temperature is defined as the mean value of the PT100 inlet and outlet temperature measurements in the further analysis.

4.4. Generation of leakage current

The focus of this thesis is the study of thermal runaway scenarios. Leakage current in the silicon sensors of the module, induced by radiation, causes the sensors to heat up, as the current is exponentially dependent on the sensor temperature. When the CO_2 cooling power is not sufficient and a certain temperature threshold is overstepped, the 2S module enters a self-heating loop, called thermal runaway. Since the 2S module in our configuration is unirradiated, the leakage current must be simulated. The method applied for this purpose was developed by Vanessa Oppenländer in Ref. [11]. This method uses LED strips to induce current on the silicon sensors, simulating an irradiated module.
The concept of the induced leakage current is to use the emitted photons of the light source to create electron-hole pairs in the silicon sensors of the 2S module. The released electrons form the generated current, which is measured with a Keithley 2410 SourceMeter [22].
The self-adhesive LED strips, placed on the cover and on top of the carbon fiber structure are aligned to the center of the 2S module so as to evenly induce current in the top and bottom silicon sensors. Both LED strips are isolated with kapton tape and powered separately by a Hameg HMP 4040 power supply [23], as can be seen in Fig. 4.7a. Each strip has twelve active LEDs, six on both the left and right side. LEDs in between, like at the U-turn, are constantly turned off by removing the resistor. The LEDs have a distance of 1.5 cm on the strip, are powered with 12 V DC, and are dimmable by regulating the applied voltage.
The power load of irradiated 2S silicon sensors is dependent on the sensors' mean temperature, according to Equation 1. Therefore the leakage current, emulated by the LEDs, has to be adjusted until the silicon sensor temperature matches the power equation. This concept is applied in a LabView program, which calculates the expected leakage current for a specific sensor temperature and adjusts the LED voltage accordingly. The variables used conform with the variables of the Ultimate@800V scenario. A proportional-integral-derivative (PID) control, implemented in the LabView program, is used to regulate and adapt the measured current to match the calculated current. The PID control calculates the difference between the measured current and the desired current, and it corrects the current using a proportional, an integrative, and a derivative term until the desired and measured current are in agreement within the desired accuracy, by adjusting the LED voltage.
The induced leakage current has to be the same for both the top and bottom silicon sensor. Since there are different spacings between the top and bottom LED strip and the silicon sensors, the top and bottom LED strips need to be operated at different voltages.
Since the employed PID algorithm is only able to regulate one process variable, the ratio of the top and bottom LED voltage for different current values is required in order to be able to control both strips with the PID control. Then one strip is used as a control variable and the second strip is powered according to the determined voltage ratio. To determine the ratio, a calibration measurement is performed, running through LED voltages between 6 and 8.5 V in 10 mV steps and measuring the induced silicon sensor current. The measurement was performed separately for the top and bottom LED.

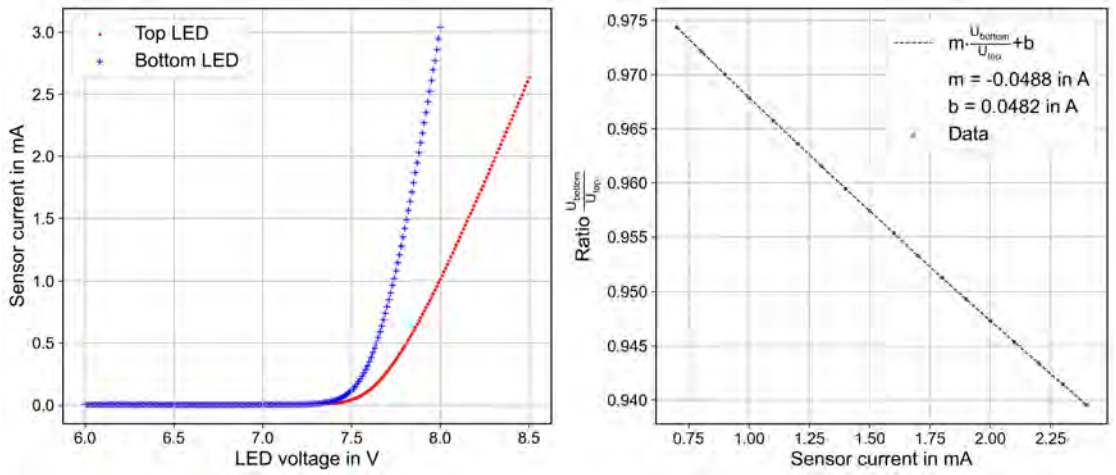

Figure 4.9: Left: result of the measurement of the sensor current against rising LED voltage. The measurements were conducted at an ambient temperature of −20 °C and with a bias voltage of 300 V. The LED voltage was increased in 10 mV steps, and the resulting current was measured after each increase. Separate measurements were performed for the top (red) and bottom (blue) LED strips on their corresponding sensor sides. Right: ratio of the bottom LED voltage divided by the top LED voltage in a current range of 0.7 to 2.3 mV. The red data points were fitted with a linear function, depicted in black.

In Figure 4.9, the results of the measurement can be seen. The induced sensor current for the bottom sensor in blue rises earlier and with a larger slope, since the distance between LEDs and bottom silicon sensor is much smaller than that between the top sensor and the cover. The bottom LED lies less than a centimeter away from the bottom silicon sensor, while the top LED is about 10 cm away from the top silicon sensor. The induced sensor leakage currents start to rise linearly at approximately 0.7 mA for both the top and bottom side. Linear functions have been fitted to the linear parts, so as to be able to calculate the ratio of the bottom voltage divided by the top voltage in 0.1 mA steps, as seen in the right plot. By fitting these data points again, an equation can be determined to calculate the required ratio for each set sensor current. The parameters for this equation have been found to $m = -0.0488\,\mathrm{A}$ and $b = 0.0482\,\mathrm{A}$. Using this method, the leakage current is evenly generated by the two sensors, half of the current is generated in the top sensor and the other half in the bottom sensor.

5. Measurement of the thermal runaway for the Ultimate@800V scenario with long inserts

Within this thesis, the thermal runaway of a 2S module with and without heating resistors on a mini-TEDD structure, cooled by two-phase CO_2, for the Ultimate@800V scenario has been measured. The 2S module is mounted on long inserts. The thermal runaway with only the 2S module active on the long inserts can be compared to thermal runaway measurements performed by Vanessa Oppenländer on short inserts [11], and to thermal simulation data of the 2S module by Nicolas Röwert [33], an ongoing doctorate in this working group. Additionally, the impact of neighboring modules, simulated with heating resistors, on the thermal behavior of the cooling structure and on the thermal runaway curve of the 2S module is investigated in the following sections.

5.1. Motivation

In the CMS experiment, sufficient cooling is vital, especially after the 2S modules have already received severe radiation. The longevity can be extended significantly with sufficient cooling.
Three radiation and operation scenarios for the HL-LHC are considered by CMS, for the purpose of this thesis, only the Ultimate@800V scenario with a 4 mm 2S module is investigated in order to examine the worst case scenario. This is reflected in the values in this scenario: after $4000\,\mathrm{fb}^{-1}$ of instantaneous luminosity the bias voltage is increased to 800 V, as compared to 600 V in the nominal scenario. The radiation damage constant increases by about 20 % to $5.14 \times 10^{-17}\,\mathrm{A/cm}$ [11]. The fluence is chosen for the location with the worst cooling conditions in the TEDD, which is in TEDD 2 on ring 11 of disk 3 [14]. The nominal fluence of $3.73 \times 10^{14}\,\mathrm{n_{eq}/cm^2}$ is 33 % increased for the Ultimate@800V scenario [11]. In the thermal runaway scenario, the temperature of a 2S module rises with a rising current. When the cooling is insufficient, it enters a self-heating loop. When a single 2S module enters thermal runaway, it also influences the neighboring modules. In a worst-case scenario, all neighboring modules could undergo thermal runaway, rendering them inoperable. Therefore it is crucial to measure the temperature at which the cooling becomes insufficient and the 2S module enters the thermal runaway, to ensure the planned cooling system enables a durable and long-lasting operation of 2S modules.

5.2. Thermal runaway measurement for one 2S module on long inserts

5.2.1. General measurement procedure

The goal of this thermal measurement is to determine the CO_2 temperature at which the 2S module starts to undergo thermal runaway. Two adjustable variables can be used to influence the silicon sensor temperature in this setup: the CO_2 cooling temperature and the induced current, because the sensor temperature depends on the current in accordance with Eq. 1. When the CO_2 temperature and the induced current on the sensor result in a stable mean sensor temperature such that

Eq. 1 is fulfilled, the system has reached an equilibrium, a so-called working point of the thermal runaway curve. Consequently, there are two methods to record the points for the thermal runaway curve. Either the CO_2 temperature is kept constant and the current gets adjusted until a working point is reached, or the induced current is kept constant and the CO_2 temperature gets adjusted. The latter method will be further explained in the following paragraph. To record the working points for the thermal runaway curve, first the targeted temperature of the 2S module silicon sensors has to be set. The ambient temperature is adjusted with the external chiller to match the set temperature within at least 0.5 K and the CO_2 is cooled down to around −30 °C. The 2S module gets powered, configured and the thresholds of the channels in the CBCs are set to the pedestal values to maximize the hybrid power consumption. Subsequently, the LEDs are turned on to induce current on the silicon sensors. The LabView program calculates the expected leakage current corresponding to the targeted silicon temperature and dims the LEDs accordingly. The last step is to adjust the CO_2 temperature in an iterative procedure until the targeted mean sensor temperature, and therefore the working point, is reached. The mean silicon sensor temperature is calculated from the seven temperature sensors on both the top and the bottom sensor. The set temperature is considered to be reached when the mean 2S module temperature agrees with the desired temperature in the first decimal place. This procedure can take up to several hours because, after a small change in the chillers or the LEDs, the whole unit needs about 30 minutes until the temperatures are in equilibrium again. When the target temperature is reached, the temperature and the power of the 2S module are recorded for several minutes. In proximity to the thermal runaway it is particularly difficult to reach a stable working point.

5.2.2. Results of the thermal runaway measurement of the 2S module

The thermal runaway measurement with a single 2S module has been conducted with the method where the sensor current is held constant, and the CO_2 temperature gets adjusted until the working point is reached. For the resulting thermal runaway curve, the silicon sensor mean temperature is plotted against the CO_2 temperature from thev PT100 sensors in the left plot in Fig. 5.1. The mean silicon sensor temperature of the 2S module ranges from −25 °C to −13 °C and is presented in blue, with systematic uncertainties of 0.3 K on the temperature sensors and approximately 0.22 K on the PT100 sensors for the CO_2 temperature. The corresponding ambient temperature is denoted by pink dots. The thermal runaway points were measured in 2 K steps in the lower temperature range and in 1 K steps near the thermal runaway approximately. Overall, an exponential curve can be observed in which the silicon sensor temperature rises increasingly rapidly at warmer CO_2 temperatures. The onset of thermal runaway occurs at approximately −29.7 °C, when the silicon sensor temperature shows a rapid increase for only small steps of the CO_2 temperature until the curve begins to bend to the left. This last measurement point is due to the employed measurement procedure and would not be present with actual irradiated 2S modules, because a stable working point is not possible in a self-heating loop. The nominal CO_2 operating temperature in the detector ranges from −35 °C to −33 °C within a cooling loop, which leaves a margin to the onset of thermal runaway of 3.3 K.

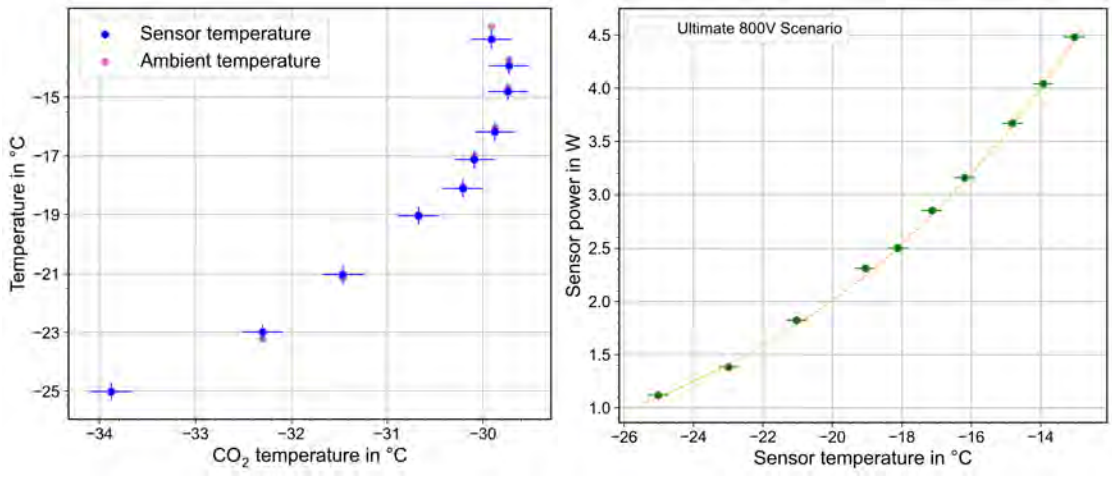

Figure 5.1: Left: thermal runaway curve for a 4 mm 2S module on long inserts in the Ultimate@800V scenario. The mean silicon sensor temperature is plotted against the CO_2 temperature in blue. The ambient temperature is depicted in pink. Right: the silicon sensor power of the 4 mm 2S module during the thermal runaway measurement. The sensor power is plotted against the sensor temperature, with the measured data shown in green and the calculated expectation for the Ultimate@800V scenario shown in yellow.

To ensure that the LED induced current is accurate, the measured sensor power of the 2S module is shown in the right plot of Fig. 5.1. The expected relation between sensor temperature and sensor current for the Ultimate@800V scenario is also depicted. The green data points have a systematic uncertainty of 0.3 K on the sensor temperature. The statistical uncertainty of the measured sensor power, determined through standard deviation calculation, is in the 1 µW scale and therefore not visible in the plot. The data points are in good agreement with the calculated sensor power and confirm the adequacy of the employed method for leakage current generation.

In the left plot of Fig. 5.2, the sensor power is plotted against the CO_2 temperature. It rises similarly to the thermal runaway curve until it reaches the upper curve limit with 4.5 W. Because the sensor power is dependent on the sensor current, which in turn correlates with the silicon sensor temperature, the shape of the curve is the same as that of the thermal runaway curve.

In the right plot of Fig. 5.2, the hybrid power plotted against the CO_2 temperature is shown, with a trend of the hybrid power being lower at low CO_2 temperatures and slightly higher at warmer CO_2 temperatures. The statistical uncertainty is about 4 µW. With an overall difference of 0.08 W, the hybrid power varies between 4.68 and 4.76 W. Although it is expected to be more or less constant, previous measurements have already demonstrated a slight temperature dependency. This could potentially be attributed to the increased efficiency of the DC-DC converters when they are cooler. Since the power differences are only on a small scale, they are considered as sufficiently constant.

In the lower plot in Figure 5.2, the power of the entire 2S module is plotted, which is the sum of the silicon sensor and hybrid power. It increases with the CO_2 temperature until it reaches the upper limit of 9.25W. The plot includes the systematic

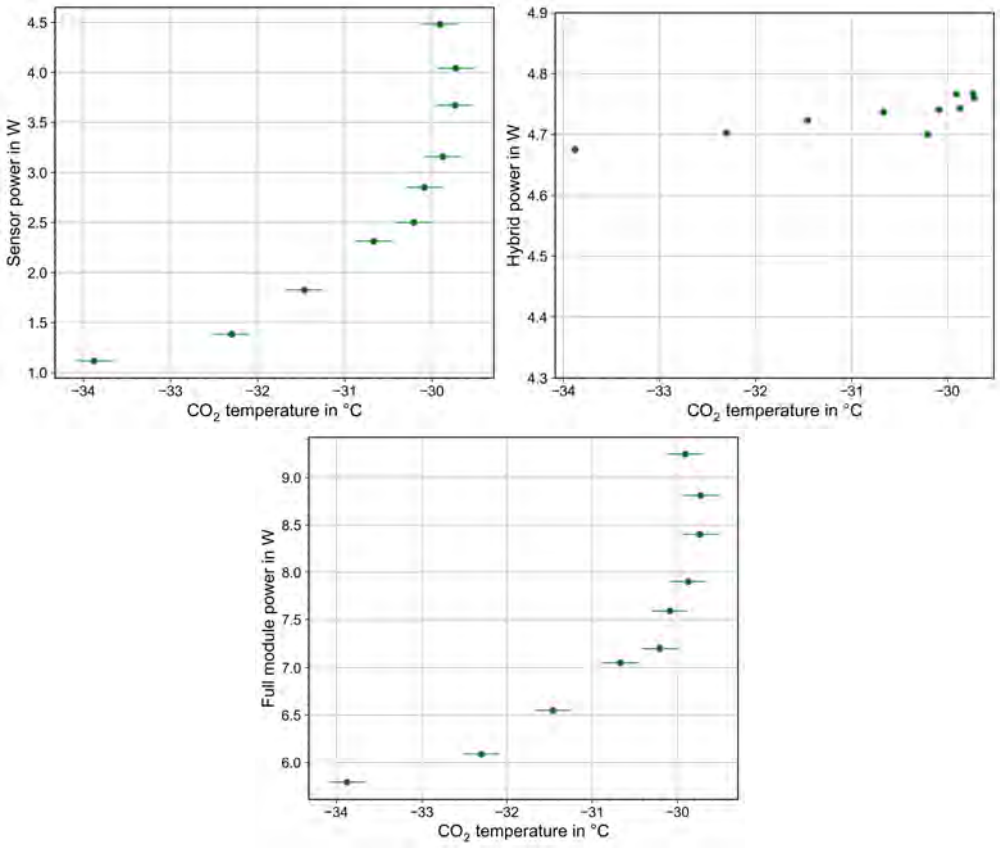

Figure 5.2: Left: silicon sensor power during the thermal runaway measurement of the 2S module in the Ultimate@800V scenario plotted against the CO_2 temperature. Right: hybrid power during the thermal runaway measurement of the 2S module in the Ultimate@800V scenario plotted against the CO_2 temperature. Below: total 2S module power during the thermal runaway measurement of the 2S module in the Ultimate@800V scenario plotted against the CO_2 temperature. The total module power is the sum of the sensor and hybrid power

uncertainty of the temperature sensors, while the statistical uncertainty, calculated by using the propagation of uncertainty with the uncertainty of the hybrid power predominating, is too small to be visible. The nominal power consumption of the entire 2S module at the nominal CO_2 temperature $-33\,°C$ is approximately 6 W in this measurement. This value will be used as the nominal power of the modules when the modules are emulated by the heating resistors.

5.2.3. Comparison to short inserts

A similar measurement with the same setup and measurement procedure using the same 4 mm 2S module was previously performed by Vanessa Oppenländer in the framework of her thesis [11], but on short inserts. One goal of this thesis was to determine the impact of long inserts compared to short inserts on the onset of thermal runaway in the Ultimate@800V scenario. For comparison, both thermal runaway curves are presented in Fig. 5.3: the left curve depicts the measurement with long inserts as already shown in Fig. 5.1, while the right curve shows the thermal runaway curve with short inserts, sourced from [11]. The pur-

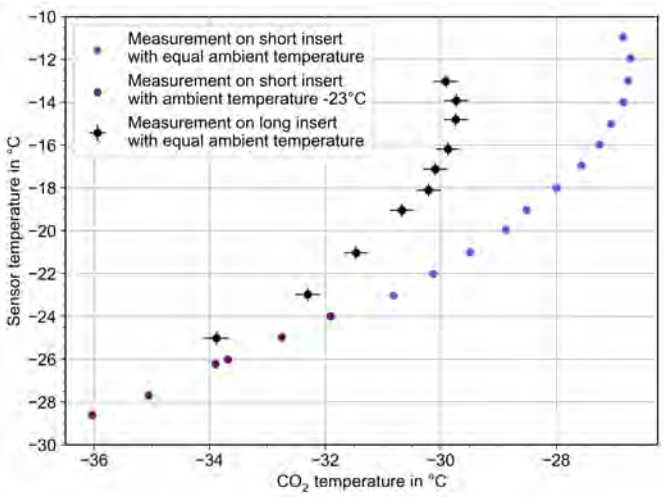

Figure 5.3: The thermal runaway curves for a 4 mm 2S module on long and short inserts, sourced from Ref. [11], in the Ultimate@800V scenario. The mean silicon sensor temperature is plotted against the CO_2 temperature. The curve for the long inserts is represented in black, while for the short inserts, it is shown in purple and blue. The blue dots represent measurements taken at an ambient temperature equaling the sensor temperature, while the purple dots represent measurements taken at a fixed ambient temperature of -23 °C.

ple data points in the plot with short inserts are taken at an ambient temperature of −23 °C because, at that time, a different chiller was used that could not go to lower temperatures. The previous setup did also not employ the built-in PT100 sensors. Therefore the CO_2 temperature was determined using the mean value of the two pressure measurements and the temperature sensors at the pipe in the mini-TEDD structure. Applying this calculation to the CO_2 temperature of the thermal runaway curve with long inserts, it results in temperatures very close to the PT100 sensor values. The temperatures above −33.5 °C match with the PT100 temperatures within 0.1 K, and only the measurement point at a CO_2 PT100 temperature of −33.9 °C deviates from the calculated −33.7 °C by 0.2 K. Consequently, the CO_2 temperatures from the thermal runaway curves on long and short inserts are well comparable.

The onset of thermal runaway on short inserts was observed at a CO_2 temperature of −27 °C, which is 2.7 K warmer compared to long inserts. The coldest point of the curve for long inserts at a sensor temperature of −25 °C is only 1 K lower compared to short inserts. While the temperature difference is just minor in the colder temperature range, the temperature differences increase with warmer CO_2 temperature. Overall, the comparison indicates that the long inserts have a noticeably inferior cooling performance compared to short inserts.

The inferior cooling performance of the long inserts in comparison to the short inserts was anticipated, but to a lesser extent. In thermal simulations for short and long inserts, the differences between the onset of thermal runaway are approximately 1 K [11, 33]. Due to their construction, long inserts possess a larger thermal resistance than short inserts, resulting in less effective heat removal. The measured thermal runaway curve is compared to simulation data in the subsequent section.

5.2.4. Comparison to thermal simulation

A thermal runaway simulation for the Ultimate@800V scenario was performed by Nicolas Röwert using a thermal model of the 2S module used in the setup. The model is based on the Finite Volume Method (FVM) and models a 2S module with 4.0 mm sensor spacing and six cooling contacts in the TEDD 2 region, as outlined in [11]. The thermal simulation has been performed using the software ANSYS [34]. The parameters for the relation of leakage current and temperature of the top and bottom sensors were taken from the Ultimate@800V scenario. The simulation considers two heat transfer coefficients (htc): $5\,\mathrm{kW/m^2/K}$ and $10\,\mathrm{kW/m^2/K}$ for the interface between the cooling pipe and the CO_2. The $5\,\mathrm{kW/m^2/K}$ is a commonly used conservative htc value, while $10\,\mathrm{kW/m^2/K}$ represents a more optimal htc value. The true htc value is difficult to determine but is assumed to lie between these two values. For each of these htc values, the sensor temperature was calculated as a function of the CO_2 temperature.
The simulation data together with the measured thermal runaway curve are shown in Fig. 5.4.
The simulation data only corresponds to sensor temperatures up to -16 °C. Beyond that point, the simulation does not converge anymore, and the onset of thermal runaway is assumed to be reached. The conservative simulation with an htc of $5\,\mathrm{kW/m^2/K}$ reaches thermal runaway at $-30.5\,°\mathrm{C}$, while the simulation with an htc of $10\,\mathrm{kW/m^2/K}$ reaches it at $-29\,°\mathrm{C}$. Therefore the two simulations yield a difference of 1.5 K. Both simulations demonstrate a shape similar to the measured thermal runaway curve, but the green curve is slightly displaced upwards and to

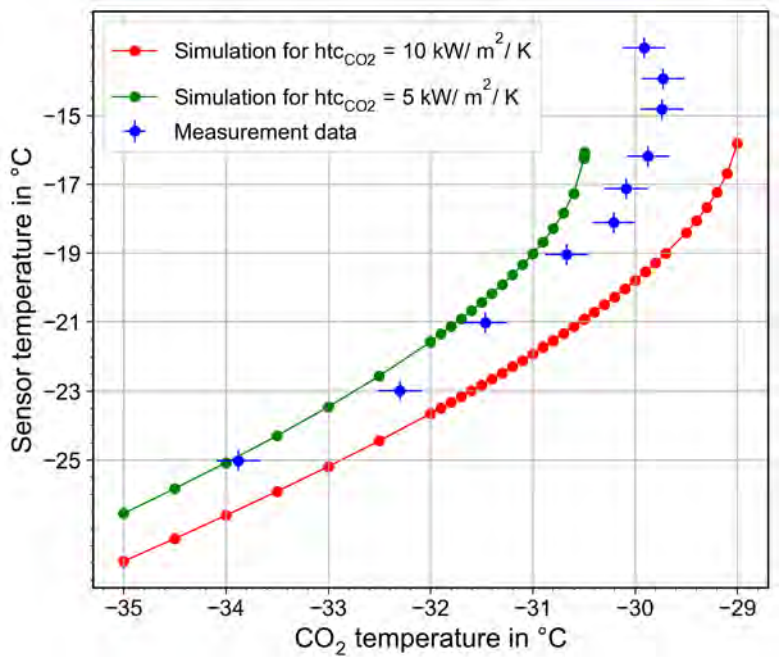

Figure 5.4: Thermal runaway curve for a 4 mm 2S module on long inserts in the Ultimate@800V scenario, with simulation data for different htc values plotted. The mean silicon sensor temperature is plotted against the CO_2 temperature in blue. Simulation data points with an htc value of $5\,\mathrm{kW/m^2/K}$ are shown in green, while those with an htc value of $10\,\mathrm{kW/m^2/K}$ are shown in red.

the left, while the red curve lies below and to the right of the measured curve. Both simulation curves reach thermal runaway at a sensor temperature of −16 °C, while the measured curve reaches it at −15 °C, 1 K warmer. The green curve fits better to the measured data, particularly at the beginning of the curve. At the onset of thermal runaway, at a sensor temperature of −16 °C, both simulation curves have a difference of approximately 0.8 K to the measured data. The measurement is therefore well in agreement with the simulations, within the uncertainties.

5.3. Effect of five neighboring modules on the thermal behavior of the cooling structure and the 2S module

This section will investigate the impact of additional neighboring modules on the heat distribution of both the cooling structure and the 2S module. Up to this point, the thermal measurements have been taken with only the 2S module active on the cooling structure. Considering that multiple 2S modules are mounted on the dees in the CMS detector, it is important to account for the effect of other neighboring 2S modules. To address this, heating resistors have been installed on the remaining five module positions of the mini-TEDD, each operated at a nominal power of 6 W per module and resulting in 1 W heat load per insert, to emulate the presence of other 2S modules.

To understand the impact of neighboring modules on the heat distribution, the heat distribution of the cooling structure with and without the heating resistors is compared in Fig. 5.5. It shows a heat map of the temperature differences at the working point with a CO_2 temperature of −33.9 °C, the mean sensor temperature of −25 °C, and 5.8 W full module power for only the 2S module powered, and the 2S module with all heating resistors powered in addition. For both measurement points, the CO_2 and ambient temperature of the working point has been used. Though the CO_2 settings have been the same for both measurements, the mean CO_2 temperature increased by approximately 0.3 K when the heating resistors were powered. This has to be considered in the comparison, and is an unaccounted effect of the CO_2 cooling system.

The squares on the heat map represent the thermistors within the mini-TEDD on the cooling pipe, while the dots indicate the thermistors mounted on the carbon fiber skin, as seen in Fig. 4.6.

The minor differences for the TEDD thermistors 1, 2, and 3 on the pipe are due to the slight change in CO_2 temperature. Additionally, the long inserts on the top side experience a temperature increase of approximately 0.9 K due to the neighboring heating resistors. The impact on the carbon fiber structure next to the module (ntm) on the upper side between the inserts (bi) on the bottom side is relatively uniform, with a difference of about 2.1 K. At the carbon fiber centers, the temperature difference is larger, reaching around 3.5 K, because of the greater distance from the cooling inserts and the cooling pipe. When the heating resistors are powered, the greatest difference is observed on the short inserts, where the temperature rises up to 4.5 K. The short inserts are anticipated to show the most significant temperature increase in this heat map when the heating resistors are activated, because the generated heat is intended to be mainly removed by the inserts and is not meant to significantly influence the cooling structure itself. The

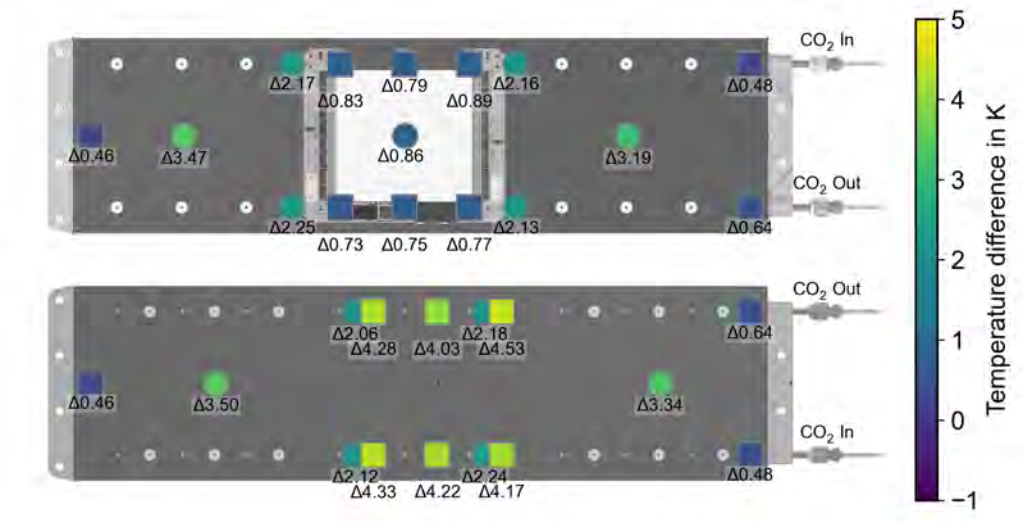

Figure 5.5: Heat map of the temperature differences of the cooling structure with a CO_2 temperature of $-33.9\,°C$ and 5.8 W full module power. The upper depiction shows the top side of the mini-TEDD structure with the mounted 2S module. The depiction below shows the bottom side. The comparison is made between only the 2S module powered and at the working point, and when all heating resistors are powered additionally. The squares represent the thermistors within the mini-TEDD on the cooling pipe and the inserts, while the dots indicate the thermistors mounted on the carbon fiber skin.

varying temperature differences among the short inserts match with their differing thermal resistances, which can vary by up to 0.5 K/W between the short inserts, as demonstrated in thermal characterization performed by Vanessa Oppenländer in Ref. [11] and reflected in the small variation of temperature differences. These different thermal resistances can be explained by differences in glue layer thicknesses [19]. Further analysis of heat distribution will be conducted in Section 6.
Figure 5.6 presents a comparison of the temperature distributions on the 2S module, showing the temperature differences at the working point at a CO_2 temperature of $-33.9\,°C$ and a mean sensor temperature of $-25\,°C$ between only the 2S module powered and when the 2S module and all heating resistors are powered. The temperature rises uniformly across the 2S module, ranging from 0.7 K to 1 K. The temperatures of the CIC and CBC are influenced the most by the heating resistors, rising by about 1 K.

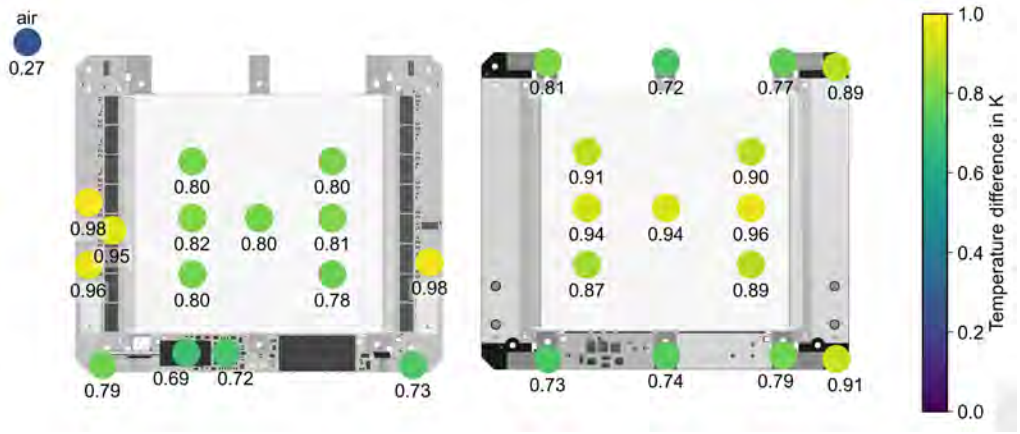

Figure 5.6: Heat map of the temperature differences on the 2S module's top side (left) and bottom side (right) the working point with a CO_2 temperature of $-33.9\,°C$ between only the 2S module powered and when the 2S module and all heating resistors are powered. The colored dots show the positions of the read out temperature sensors and the temperature differences in K are indicated.

The same comparison has been performed at a working point with a CO_2 temperature of $-29.7\,°C$ and a mean sensor temperature of $-15\,°C$ with 8.4 W full module power. The heat map in Fig. 5.7 demonstrates the differences between only the 2S module powered and when the 2S module and all heating resistors are powered. The temperature differences for the cooling structure and the 2S module are very similar to the one at $-33.9\,°C$ CO_2 temperature. This consistency suggests that the influence of the heating resistors remains uniform across different silicon sensor temperatures.

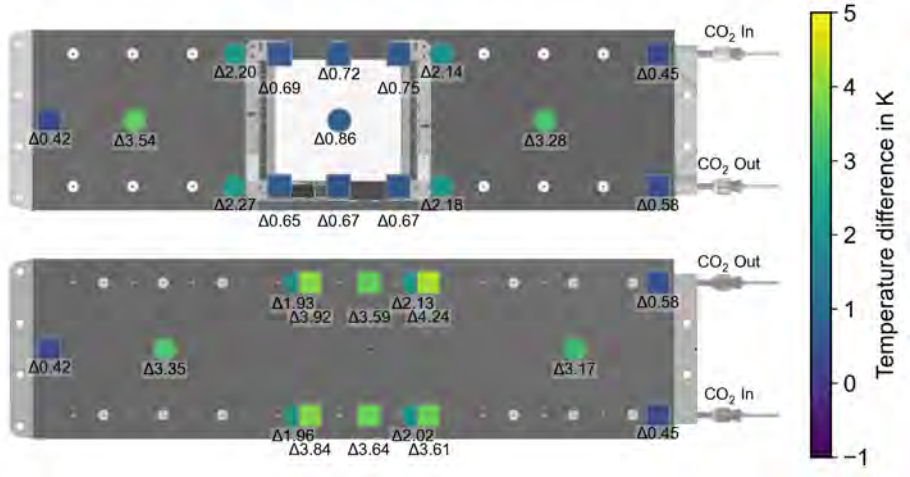

Figure 5.7: Heat map of the temperature differences at a CO_2 temperature of $-29.7\,°C$ and 5.8 W full module power. The upper depiction shows the top side of the mini-TEDD structure with the mounted 2S module. The depiction below shows the bottom side. The comparison is made between only the 2S module powered and at the working point, and when all heating resistors are powered additionally. The squares represent the thermistors within the mini-TEDD on the cooling pipe and the inserts, while the dots indicate the thermistors mounted on the carbon fiber skin.

As demonstrated, the heating resistors significantly impact the heat distribution on the cooling structure and the 2S module. Therefore, the subsequent section repeated the thermal runaway measurement with emulated neighboring modules to investigate their impact on the onset of thermal runaway.

5.4. Results of the thermal runaway measurement for the 2S module and neighboring modules

5.4.1. Results of the thermal runaway measurement

The measurement procedure to obtain the thermal runaway curve with the 2S module mounted on long inserts and five heating resistors is slightly different than the procedure used before[2]. The points have been recorded with the small difference that the heating resistors were powered before the 2S module was turned on. The measured curve can be seen in the left plot of Fig. 5.8. The onset of thermal runaway is observed at the CO_2 temperature of $-30.4\,°C$. The ambient temperature of the second point at $-33.6\,°C$ CO_2 temperature does not match exactly with the sensor temperature, but that does not affect the onset of the thermal runaway. In the right plot, the measured sensor power of the 2S module is shown in green. In yellow, the expected relation between sensor temperature and sensor leakage current for the 800V Ultimate scenario is shown, which again confirms the adequacy of the employed method for leakage current generation The sensor and hybrid power measurements have been examined, but show no considerable difference to the power distribution for only the 2S module powered.

[2]The two coolest working points have been found with the CO_2 temperature held constant, while the sensor current has been adjusted until the working point was reached and the sensor temperatures were in equilibrium.

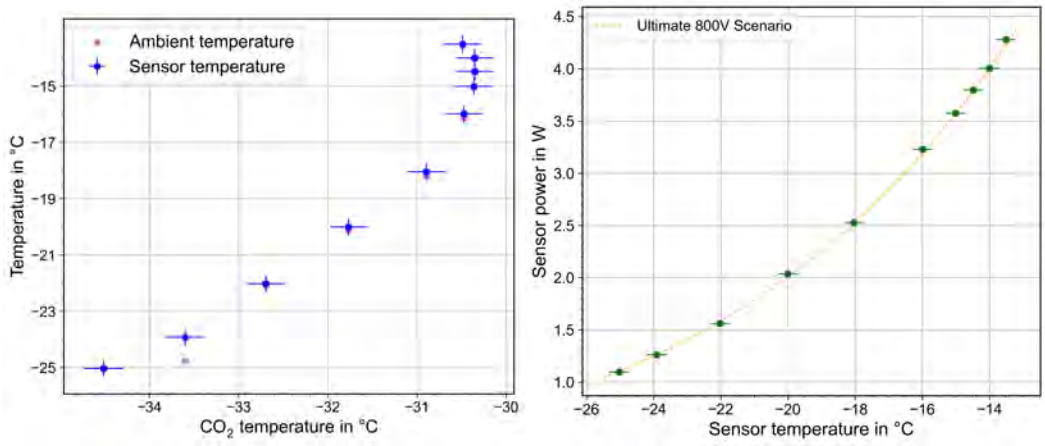

Figure 5.8: Left: silicon sensor power during the thermal runaway measurement of the 2S module and five heating resistors at the Ultimate@800V scenario plotted against the CO_2 temperature in blue. The corresponding ambient temperature is shown in pink. Right: the sensor power during the thermal runaway measurement of the 2S module and five heating resistors at the Ultimate@800V scenario plotted against the CO_2 temperature.

5.4.2. Comparison to 2S module on long inserts and simulation data

The effect of the emulated 2S modules can be seen in the comparison of the thermal runaway curve of the 2S module alone on long inserts and the curve with the additional heating resistors powered. Notably, the thermal runaway curve with the 2S module and heating resistors show a similar shape to the curve with only the 2S module powered, but is shifted to the left, with the thermal runaway beginning 0.8 K earlier. As shown in Fig. 5.9, the new thermal runaway curve closely aligns with the simulation data employing an htc of 5 $kW/m^2/K$. However, this does not directly imply that the htc of 5 $kW/m^2/K$ is the correct htc for the setup, since it cannot be distinctly determined. The effect of the heating resistors cannot be directly correlated to the simulation, which does not account for the potential impact of the cooling structure or neighboring modules. But it allows the interpretation that the cooling structure supports the cooling of the 2S module, which could be compensated for by the neighboring modules. This idea cannot be distinctly assessed with the present data.
This earlier onset of thermal runaway leaves an even smaller margin of 2.5 K to the nominal CO_2 temperature before the onset of thermal runaway. Despite the potentially less effective cooling of the long inserts compared to the short inserts, it can be observed that the heating resistors have a significant impact on the 2S module and the onset of thermal runaway. This measurement has been performed for a worst-case scenario and the 2S module with the highest fluence in the TEDDs. Therefore, the remaining margin for other modules at different locations in the detector will be larger.

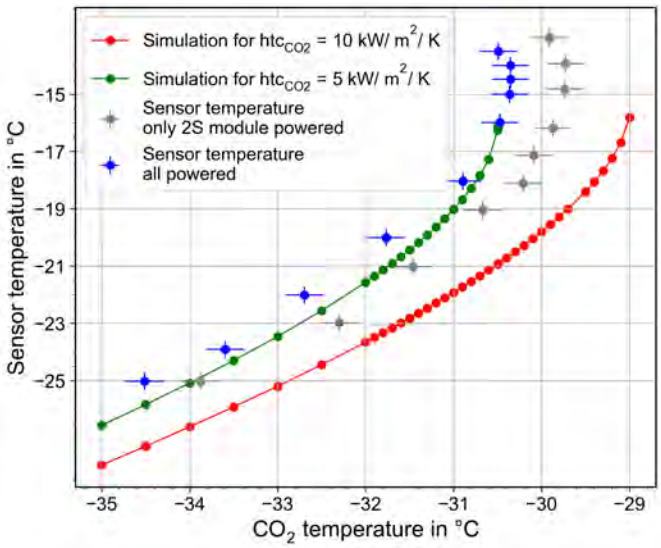

Figure 5.9: Silicon sensor power during the thermal runaway measurement of the 2S module and five heating resistors at the Ultimate@800V scenario plotted against the CO_2 temperature in blue.The measured thermal runaway curve with only the 2S module powered is shown in grey for comparison. Simulation data points with an htc value of 5 $kW/m^2/K$ are shown in green, while those with an htc value of 10 $kW/m^2/K$ are shown in red. Right: the sensor power during the thermal runaway measurement of the 2S module and five heating resistors at the Ultimate@800V scenario plotted against the CO_2 temperature.

6. Investigation of the heat flux on the cooling structure

In this section, the heat flux on the mini-TEDD cooling structure is analyzed in greater detail. The influence of modules mounted on both the top and bottom sides on the inserts of the cooling structure and on the carbon fiber surface is surveyed using temperature sensors. This is done to understand how the neighboring modules impact the thermal behavior of the 2S module.

6.1. Motivation

In the previous section, the influence of neighboring modules on the onset of thermal runaway of the 2S module on long inserts was observed to be a reduction by 0.8 K. To analyze the effect that the neighboring modules have on the thermal management of the 2S module, the temperature distribution of the cooling structure is further investigated, examining potentially significant heat flow to the CO_2 pipe and to the carbon fiber skin. Therefore, thermal measurements with different configurations of powered 2S modules and emulated modules have been performed. In the first configuration, the thermal behavior of the mini-TEDD structure with only the 2S module activated in the top center position on long inserts is compared to the thermal behavior with only the emulated module activated on the bottom center position. For the second configuration, the thermal behavior with all real and emulated modules powered on the top side is compared to all emulated modules powered on the bottom side. In the third and last configuration, the thermal behavior with only the 2S module activated is compared with the thermal behavior when the left and right emulated modules on the bottom side are additionally activated. These additional emulated module positions have been selected as they are furthest away from the 2S module, spatially.

6.2. Results and comparison of one module powered on the top/bottom center position

In this thermal measurement procedure, the first step was to adjust the setup to the working point of the thermal runaway curve of the 2S module on the top center position for a sensor temperature of $-25\,°C$ and a CO_2 temperature of $-33.9\,°C$, corresponding to a full module power of 5.8 W. After several minutes of measurement, the 2S module was deactivated and the emulated module on the bottom center position is turned on. At last, the emulated module was turned off to measure the heat distribution with all modules turned off with ambient and cooling conditions matching those of the working point of the thermal runaway curve at the CO_2 temperature of $-33.9\,°C$. The results of the three measurements are shown in Fig. 6.1. Every temperature value has a systematic uncertainty of 0.3 K and a negligible small statistical uncertainty.
It is observed that the average temperature of the green squares on the left plot is higher, around -29 K, compared to the average temperature of -29.8 K of the blue dots on the right plot. This slight difference in behavior is expected since the heating resistors emulate a module power of 6 W, whereas the full power of the

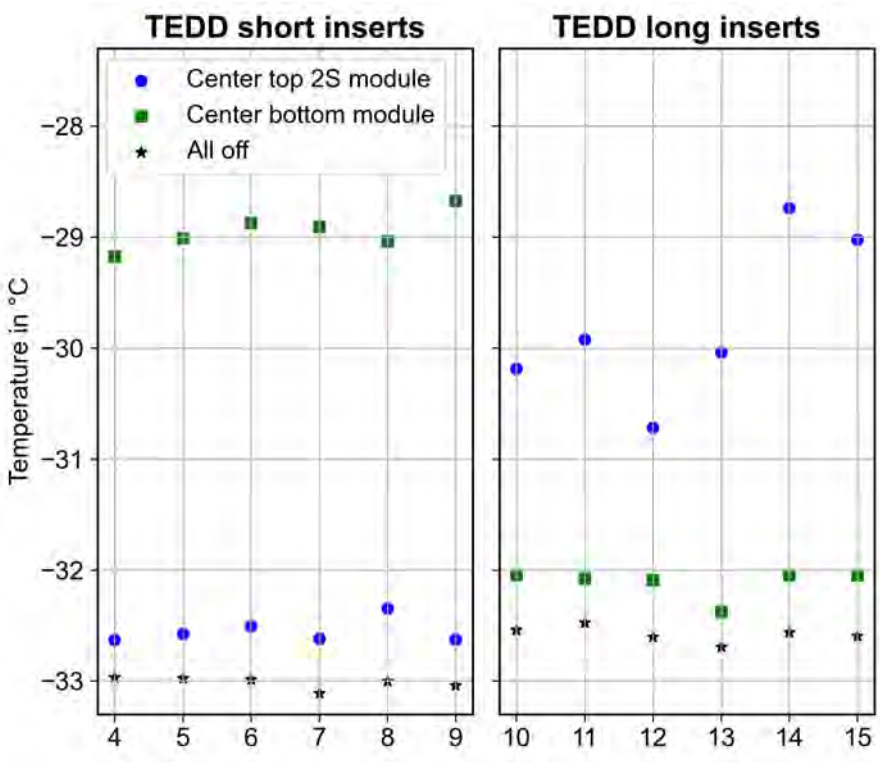

Figure 6.1: Values of the temperature sensors glued to the inserts for the 2S module activated in the top center position in blue, the emulated module activated in the bottom center position in green, and the temperature values when everything is turned off in black. The left plot displays the temperature values of the temperature sensors glued to the short inserts within the mini-TEDD structure, while the right plot shows the temperature values of the long inserts. The ambient and CO_2 temperature are adjusted to the working point at a CO_2 temperature of $-33.9\,°C$ and 5.8 W full module power.

2S module is 5.8 W for this CO_2 temperature of $-33.9\,°C$. This small difference can result in temperature of up 1 K, according to the right plot in Fig. 5.1 The blue dots on the right plot form a pattern corresponding to the heat distribution on the 2S module. Inserts 14 and 15 are the warmest as they are closest to the DC-DC, which is responsible for almost 1.8 W of the whole 2S module power alone [3]. However, this pattern is not clearly transferred to the short inserts, shown in the blue dots on the left plot. Although each heating resistor puts 1 W into each insert, the heat distribution is influenced by the thermal resistance of the inserts, resulting in the depicted pattern of the green squares on the left plot. For example, insert 9 has the highest thermal resistance with 2.43 K/W at a CO_2 temperature of $+15\,°C$ [11] and is the warmest insert out of the short inserts in most measurements.However, the systematic uncertainty of 0.3 K does not allow distinct conclusions for the small pattern differences. The influence on the long inserts can be seen by examining the green squares in the right plot. The temperature drop of insert 13 could also be due to its thermal resistance, but only the short inserts have been characterized individually in Ref.[11].

The module positions on the top side and the bottom side of the cooling structure are shifted relative to each other. Each opposite-facing position has two inserts with neighboring inserts to the left and right on the north and south side, and one

insert with only one neighbor. The thermistors 4 and 9 are inserts with only one neighbor, whereas 5, 6, 7, and 8 have two neighboring long inserts. If the heat load is directly transferred between the inserts, it could be possible that the inserts with only one neighbor insert behave warmer or colder than the inserts with two neighbors. However, neither inserts 4 and 9 nor 10 and 15 demonstrate such a behavior.

It is also interesting to see that the temperature difference of 0.5 K between the blue points and all off on the left plot is practically equal to the difference between the green squares and all off on the right plot. This suggests that the influence of the top 2S module on long inserts to the neighboring short inserts is the same as the influence of the bottom emulated module on short inserts to the neighboring long inserts. Therefore, although individual inserts do not appear to influence the temperature of their neighboring inserts, the consistent impact of the 2S module on the short inserts and of the emulated module on the long inserts suggests an additional uniform heat flux via the CO_2 pipe.

Regarding the black stars in Fig. 6.1, it is notable that the short inserts are approximately 0.5 K cooler than the long inserts when everything is turned off. This new observation contrasts with previous measurements conducted by Vanessa Oppenländer [11], where the 2S module was mounted on short inserts on the top side. In that configuration, the insert temperatures were nearly equal when the 2S module was deactivated, with only a small trend of the long inserts being slightly colder by about 0.1 K [11], explainable within the systematic uncertainties.

In that context, significant differences in the thermal behavior of the cooling structure and the deactivated 2S module mounted on long inserts have been observed in comparison to the 2S module mounted on short inserts. In the setup with the 2S module on short inserts in Ref.[11], the measurement with a deactivated 2S module was performed at a CO_2 temperature of $-33.1\,^{\circ}\mathrm{C}$ and an ambient temperature of $-22.6\,^{\circ}\mathrm{C}$, resulting in a mean sensor temperature of $-32\,^{\circ}\mathrm{C}$. A similar measurement on the present setup with the deactivated 2S module mounted on long inserts at a colder CO_2 temperature of $-33.9\,^{\circ}\mathrm{C}$ and an ambient temperature of $-25\,^{\circ}\mathrm{C}$ resulted an approximately same mean sensor temperature of $-32.1\,^{\circ}\mathrm{C}$. The temperature difference to the CO_2 temperature for the short inserts is 1.1 K and for the long inserts 1.8 K. In the present setup, a colder CO_2 temperature and a colder ambient temperature result in the same mean sensor temperature for long inserts than warmer CO_2 and ambient temperature on short inserts. A possible explanation is that the temperature of the area of the deactivated 2S module adapts to the ambient temperature. Since the short inserts cool more effectively than the long inserts, the same sensor temperature can be achieved with a warmer CO_2 and ambient temperature for short inserts than for long inserts.

The influence of the ambient temperature on the deactivated 2S module temperature can be a possible explanation for the temperature difference of 0.5 K between long and short inserts in the present setup and the minimal difference in the setup with the 2S module mounted on short inserts in Ref.[11]. Cooled dry air exits the vents directly under the mini-TEDD structure. Ambient temperature measurements suggest a slightly cooler ambient temperature below the mini-TEDD compared to on top of it, by less than 1 K. Because the 2S module has a larger

area compared to the emulated modules to adapt to the ambient temperature, the inserts with the 2S module mounted always receive more heat load than the inserts without the 2S module. The more effective cooling of the short inserts compared to the long inserts, coupled with the assumed small ambient temperature difference between the top and bottom sides, likely results in the temperature difference of 0.5 K in the present setup and almost no temperature difference when the 2S module is mounted on short inserts in Ref. [11].

In Figure 6.2, the temperature values of the thermistors on the carbon fiber surface for the same thermal measurement as before can be seen. The left plot shows the thermistors on the bottom side, mounted between the short and long inserts (bi) on the carbon fiber skin. The right plot shows the thermistors mounted left and right next to the 2S module (ntm) on the top side, as seen in Fig. 4.6.

The black stars show that the bottom side is again cooler than the top side by 1 K. The main reason for this behavior is assumed to be the location of the CO_2 pipe, which is very close to the bottom side as demonstrated in Fig. 4.3, and therefore is cooling it more. Minor additional reasons could be that air is trapped below

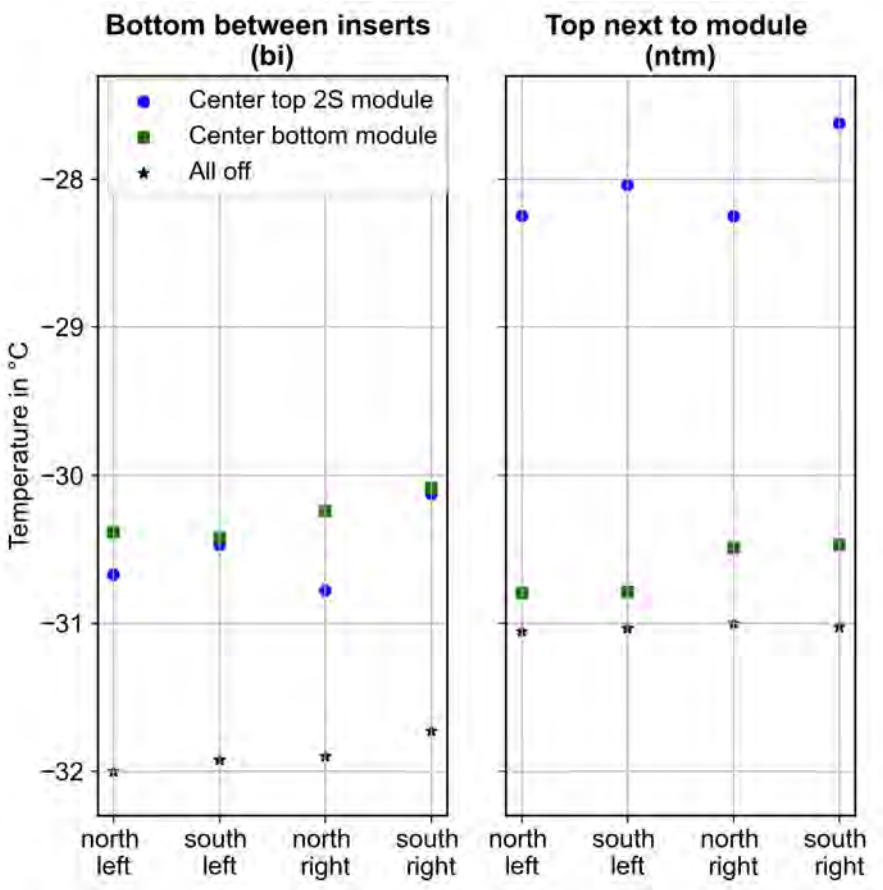

Figure 6.2: Values of the temperature sensors mounted on the carbon fiber surface of the cooling structure for the 2S module activated in the top center position in blue, the emulated module activated in the bottom center position in green, and the temperature values when everything is turned off in black. The ambient and CO_2 temperature are adjusted to the thermal runaway curve point with a CO_2 temperature of −33.9 °C and 5.8 W full module power.

the mini-TEDD cooling structure, with cooled air straight from the vents, which is colder than the average ambient temperature, and that the bi thermistors are closer to the inserts than the ntm thermistors, spatially.
The comparison of the blue dots on the left plot with the green squares on the right plot indicates that the 2S module influences the temperature measured by the bottom bi thermistors by about 1 K stronger, than the emulated module on the bottom center position influences the temperature measured by the top ntm thermistors. The green squares on the left plot and the blue dots on the right plot demonstrate that the emulated module on the bottom center position increases the temperature measured with the bi thermistors by about 0.5 K, while the 2S module increases the temperatures measured by the ntm thermistors by about 1.5 K.
This behavior could be caused by the fact that the long inserts protrudes out from the carbon fiber skin on both the top and bottom side. Therefore the heat that is transferred off of the 2S module via the long inserts has a direct path to influence the carbon fiber skin on the bottom. The short inserts however are shielded from the top side with an insert support made out of a plastic material, as demonstrated in Fig. 4.3. This insert support could possibly prevent the heat transfer from the short insert to the top carbon fiber skin layer.
The green squares on the left plot show a uniform distribution, influenced by the pattern of the measurement in black. The pattern of the green squares on the right plot shows a different behavior for the left and right side. A reasonable cause for this behavior could be that the bottom center position is shifted to the right in comparison to the top center position.
The blue dots in the right plot form a pattern according to the heat distribution on the 2S module, the south is warmer because the service hybrid is located in the south; the right south position is close to the DC-DC convertersand therefore even warmer. The pattern is transferred to the location of the bi thermistors and can be seen in the left plot, too.
This strongly suggests a considerable additional heat flux between the inserts and the carbon fiber surface as well as between the two carbon fiber surfaces via the the long inserts.

The measurements have also been realised in two different configurations, with all real and emulated modules on the top or the bottom side powered, and also the 2S module with two additional powered emulated modules on the left and right bottom position. The corresponding plots can be found in the Appendix in Fig. A.4-A.7. These measurement do not reveal any new or different insights, the behavior is very similar but with larger temperature differences. The heat flux on the carbon fiber skin will be further investigated in the following, for all three configurations.

6.3. Results and comparison of the heat flux on the carbon fiber center

The thermistors on the carbon fiber center are positioned furthest away from the inserts and CO_2 pipe, making them suitable for investigating the heat flux on the carbon fiber surface. Their exact positions and labels can be seen in Fig. 4.6.

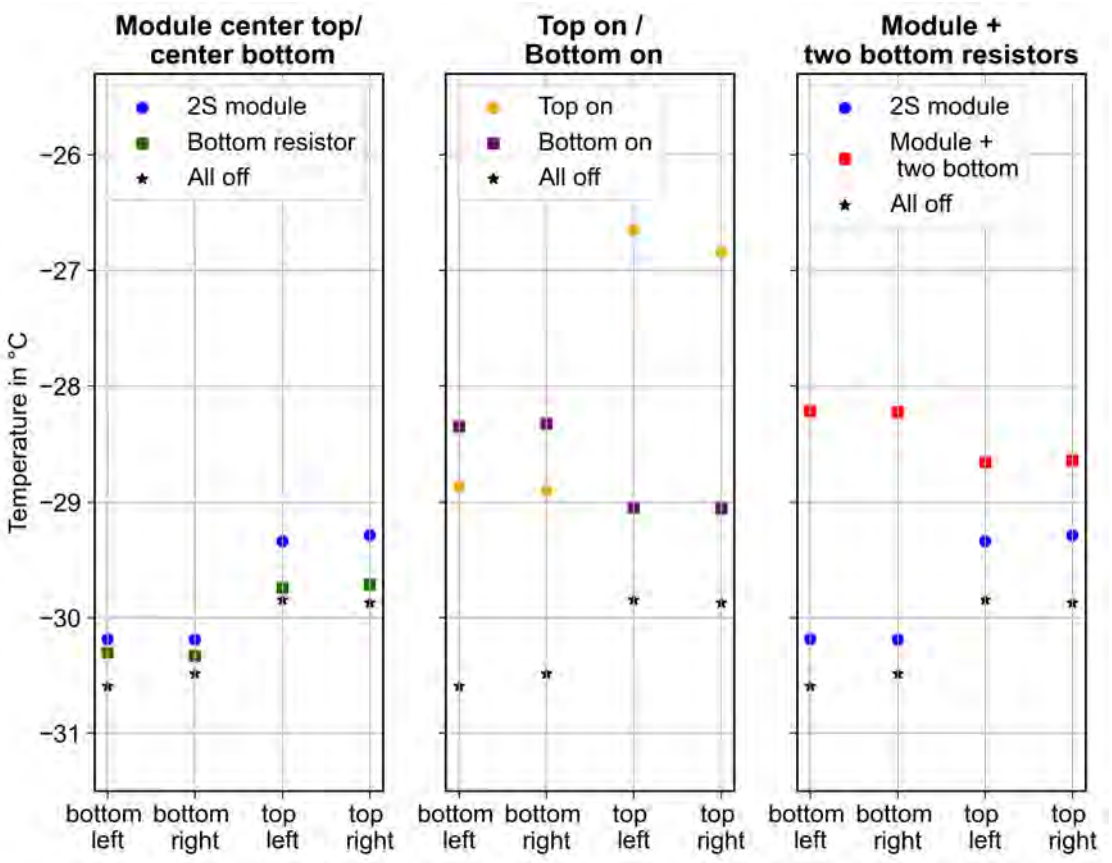

Figure 6.3: Values of the temperature sensors mounted on the carbon fiber surface of the cooling structure in the carbon fiber center position. The left plot shows the 2S module activated on the top center position in blue, and the emulated module activated on the bottom center position in green. The middle plot shows the top side activated in yellow and the bottom side activated in purple. In the right plot, the 2S module activated on the top center position is shown in blue, and with two additional bottom modules activated on the left and right in red. The temperature values when everything is turned off are depicted in black. The ambient and CO_2 temperature are adjusted to the thermal runaway curve point with a CO_2 temperature of $-33.9\,°C$ and 5.8 W full module power.

The carbon fiber center temperature values have been recorded in three configurations and are presented in Fig. 6.3. In the left plot, temperature values from the first configuration are displayed, where only the 2S module is activated in the top center position on long inserts or only the emulated module is activated on the bottom center position. The middle plot showcases the second configuration, where all modules are activated on either the top side or the bottom side. The right plot shows the third configuration, where the 2S module is activated with emulated modules on the left and right bottom side additionally activated.

The left plot in Fig. 6.3 displays the temperature values with only the 2S module activated in the top center position on long inserts and only the emulated module activated on the bottom center position. The 2S module increases the temperature of the neighboring center positions on the top side by about 0.5 K, with a slightly lesser effect on the bottom center positions. The emulated module on the bottom side exerts a minimal impact of about 0.2 K on the neighboring center positions on

the left and right bottom side, and about the same effect on the positions on the top side. The same behavior is observed in the middle plot for the entire top side or the entire bottom side activated, but with larger temperature differences, as the thermistor center positions are located directly between the activated heating resistors. The influence of the powered emulated modules on the center position in the third configuration is depicted in the right plot. The blue dots represent the temperature with only the 2S module activated, while the red dots indicate the additional activation of two emulated modules on the left and right bottom side. These emulated modules increase the temperature on the bottom side by approximately 2 K and by about 0.7 K on the top side.
Overall, the presence of neighboring modules causes a significant increase in the carbon fiber surface temperature, suggesting a significant heat flux via the carbon fiber. This heat flux is likely responsible for the earlier onset of thermal runaway with neighboring modules by 0.8 K.

7. Summary

The 2S module is a substantial part of the Phase-2 upgrade for the CMS tracker. This thesis investigated the thermal behavior of the 2S module mounted on the aluminum cooling contacts of the TEDD in the endcaps. With proceeding irradition, the silicon sensors within the 2S module experience increasing leakage current, directly impacting the sensor temperature. If the cooling power is not sufficient, the 2S module can enter a self heating loop: the thermal runaway. In this thesis, a 4 mm 2S module is mounted on the long inserts of a mini-TEDD cooling structure, which is placed inside an actively cooled box to prevent thermal exchange with the environment. New CO_2 temperature sensors have been integrated into the CO_2 pipe, providing accurate CO_2 temperature measurements. The LED strips have been calibrated to induce the expected current on the silicon sensors for a targeted mean sensor temperature.
Thermal runaway measurements were conducted with the 2S module mounted on the long inserts of the mini-TEDD, with heating resistors emulating six neighboring modules for the Ultimate@800V scenario. Thermal runaway with only the 2S module activated begins at a CO_2 temperature of $-29.7\,°C$, which leaves a margin of 3.3 K to the expected maximal CO_2 temperature along a cooling loop. It is compared to the measured thermal runaway curve of the same 2S module on short inserts, performed by Vanessa Oppenländer [11], which resulted in the insight that the thermal runaway curve of the long inserts starts 3 K earlier than for the short inserts. For the thermal runaway with neighboring modules, the onset is shifted by 0.8 K to lower temperatures, providing less than 2.5 K margin. The thermal runaway simulation data provided by Nicolas Röwert [33] aligns well with the measured curve. In addition, thermal measurements regarding the heat flux on the mini-TEDD structure were conducted, to explore how neighboring modules impact the thermal behavior of the 2S module. The conclusion is that these additional modules induce a significant uniform heat flow onto both the CO_2 pipe and the carbon fiber. The long inserts establish a thermal connection between the top and bottom sides, potentially supporting the cooling effect on the side with short inserts.
The performance of additional thermal runaway measurements with six 2S modules would be interesting to verify if the heating resistors effectively emulate a 2S module. Additionally, conducting further thermal measurements with different powered module configurations could provide a deeper understanding of the heat flux on the test cooling structure.

References

[1] CMS Collaboration, *Observation of a new boson at a mass of 125 GeV with the CMS experiment at the LHC*, https://doi.org/10.1016/j.physletb.2012.08.021, Phys. Lett. B 716 30-61, 2012.

[2] ATLAS Collaboration, *Observation of a new particle in the search for the standard model Higgs boson with the ATLAS detector at the LHC*, https://doi.org/10.1016/j.physletb.2012.08.020, Phys. Lett. B 716 1–29, 2012.

[3] CMS Collaboration, *The Phase-2 Upgrade of the CMS Tracker, CERN-LHCC-2017-009*, 2017, DOI: 10.17181/CERN.QZ28.FLHW.

[4] O. Brüning et al, *The scientific potential and technological challenges of the High-Luminosity Large Hadron Collider program*, Rep. Prog. Phys. 85 046201, 2022, DOI: 10.1088/1361-6633/ac5106.

[5] CERN, *Accelerating: Radiofrequency cavities*, URL: https://home.cern/science/engineering/accelerating-radiofrequency-cavities.

[6] CERN, *LHC Run 3: physics at record energy starts tomorrow*, 2022, URL: https://home.cern/news/news/physics/lhc-run-3-physics-record-energy-starts-tomorrow.

[7] CERN, *Longer term LHC schedule*, 2022, URL: https://lhc-commissioning.web.cern.ch/schedule/LHC-long-term.htm.

[8] T. Sakuma and T. McCauley, *Detector and Event Visualization with SketchUp at the CMS Experiment*, J. Phys.: Conf. Ser. 513 022032, 2019, DOI: 10.1088/1742-6596/513/2/022032.

[9] The CMS Collaboration et al, *The CMS experiment at the CERN LHC*, JINST 3 S08004, 2008, DOI: 10.1088/1748-0221/3/08/S08004.

[10] CMS Collaboration, *Public CMS Luminosity Information*, URL: https://twiki.cern.ch/twiki/bin/view/CMSPublic/LumiPublicResults#2024_proton_proton_collisions_at.

[11] V. Oppenländer, *Thermal Measurements with a 2S Module on a TEDD-like Structure for the CMS Phase-2 Upgrade*, RWTH Aachen University, MSc Thesis, 2023.

[12] N. Röwert, *CAD Drawings*, private communication, 2023.

[13] The Tracker Group of the CMS Collaboration, *Selection of the silicon sensor thickness for the Phase-2 upgrade of the CMS Outer Tracker*, JINST 16 P11028 (2021), DOI: 10.1088/1748-0221/16/11/P11028.

[14] G. Bianchi et al., *Irradiation Outer Tracker*, URL: https://ghugo.web.cern.ch/ghugo/layouts/test/OT616_IT613_power/irradiation_Outer.html.

[15] F. Hartmann, *Evolution of Silicon Sensor Technology in Particle Physics*, Springer, 2017, DOI: 10.1007/978-3-319-64436-3.

[16] G. Baldinelli et al., *The Tracker End-Cap Double Disks (TEDD) of the CMS Phase 2 Outer Tracker*, private communication, 2023.

[17] *CMS working group at DESY*, URL: https://desy-cms.desy.de.

[18] F. Scholz, *Untersuchung der Eigenschaften eines CO2-Kühlsystems für das Upgrade des CMS-Spurdetektors*, RWTH Aachen University, BSc Thesis, 2012.

[19] M. Rauch, *Thermal Measurements and Characterizations for the CMS Phase-1 Barrel Pixel Detector and the CMS Phase-2 Upgrade Tracker 2S Module with Evaporative CO2 Cooling Systems*, RWTH Aachen University, PhD Thesis, 2020.

[20] O. Reichelt, *2S Thermal Test Structure*, private communication, 2022.

[21] Tektronix, *Keithley 2701 Multimeter*, URL: http://lns00.psi.ch/sinqwiki/attach?page=MissingSamEnvDocumentation%2Fkeithley-2701-900-01B.pdf.

[22] Tektronix, *Keithley 2410 SourceMeter*, URL: https://www.tek.com/de/products/keithley/source-measure-units/2400-standard-series-sourcemeter.

[23] Rohde & Schwarz, *HMP4040*, URL: https://www.rohde-schwarz.com/de/produkte/messtechnik/dc-netzgeraete/rs-hmp4000-netzgeraeteserie_63493-47360.html.

[24] TE connectivity, *Micro BetaCHIP (MCD) Thermistor Probe*, URL: https://www.te.com/de/product-CAT-NTC0065.html.

[25] HUBER, *CC 505 refrigeration bath circulator*, URL: https://www.huber-online.com/en/products/baths-and-circulators/cooling-heating-circulators/cc-modelle-bis-90c/cc-505.

[26] IST, *HYGROCHIP Humidity Sensor LabKit*, URL: https://www.ist-ag-japan.com/brand2/pdf/HYT-271.pdf.

[27] Swagelok, *Double Ended Sample Cylinder*, URL: https://products.swagelok.com/en/c/dot-compliant-cylinders/p/304L-HDF4-1GAL.

[28] Hanning, *VARICON Three-phase Motor*, URL: https://www.all-electronics.de/wp-content/uploads/migrated/document/158069/57c643481cb.pdf.

[29] HUBER, *Unistat 815 Circulation Thermostat*, URL: https://www.huber-online.com/produkte/dynamische-temperiersysteme/unistate-bis-120c/unistat-815-2.

[30] National Instruments, *LabView Graphical Programming Environment*, URL: https://www.ni.com/de/shop/labview.html.

[31] *PT100 sensor*, URL: https://www.electronic-sensor.de/widerstandsthermometer/widerstandsthermometer-swagelok.

[32] B. Wischnewski, *CO2 Calculator*, URL: https://www.peacesoftware.de/einigewerte/co2.html.

[33] N. Röwert, *Thermal runaway simulation data*, private communication, 2023.

[34] *Thermal Analysis Software ANSYS*, URL: https://www.ansys.com/applications/thermal-analysis-simulation-software.

A. Appendix

A.1. CO_2 cooling setup

In the following a photo of the CO_2 cooling system, and the mounted PT100 sensors can be found, as well as a schematic overview of the CO_2 cooling circuit.

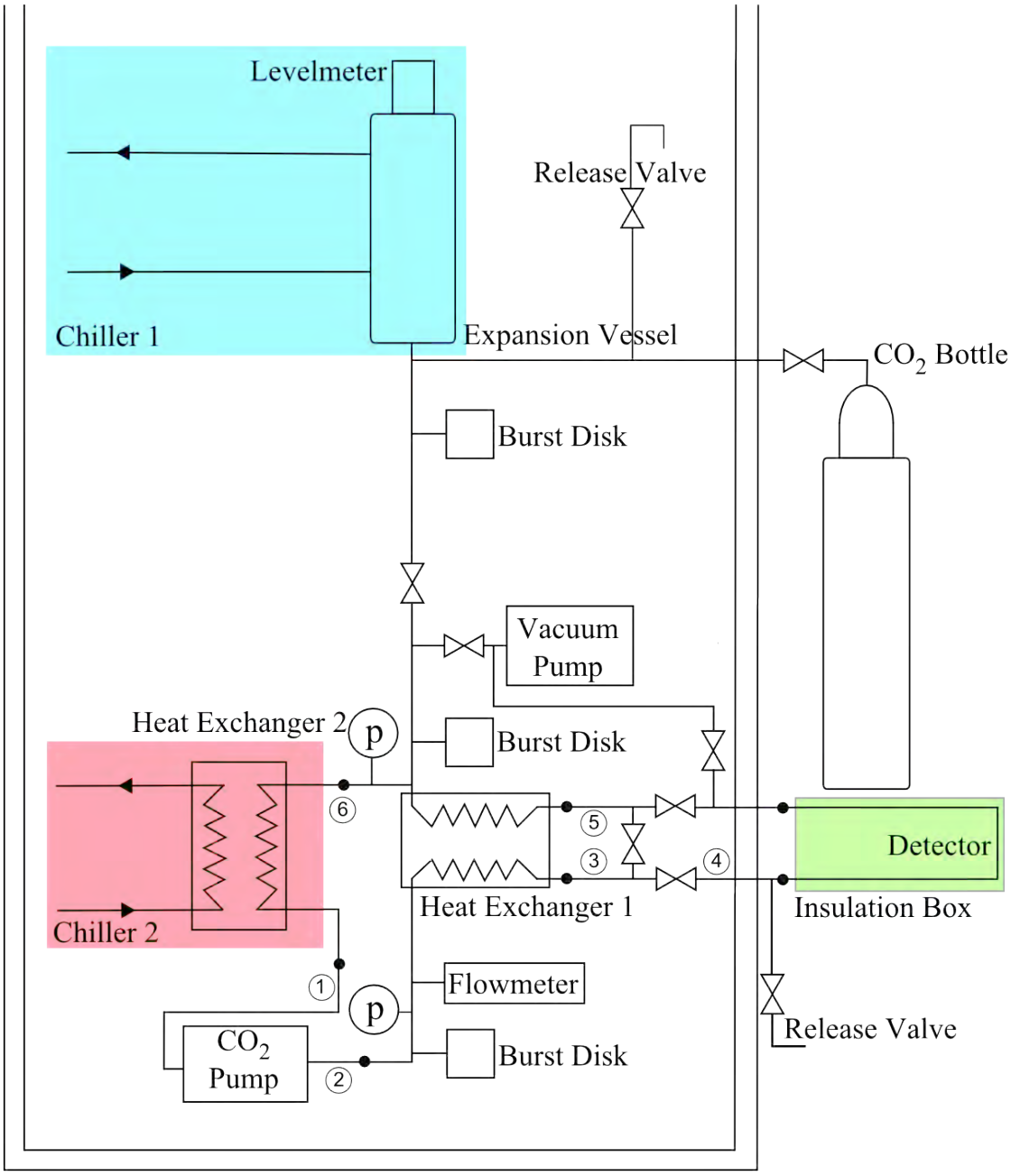

Figure A.1: Schematic overview of the CO_2 cooling circle.

Figure A.2: Photo of the CO_2 cooling system.

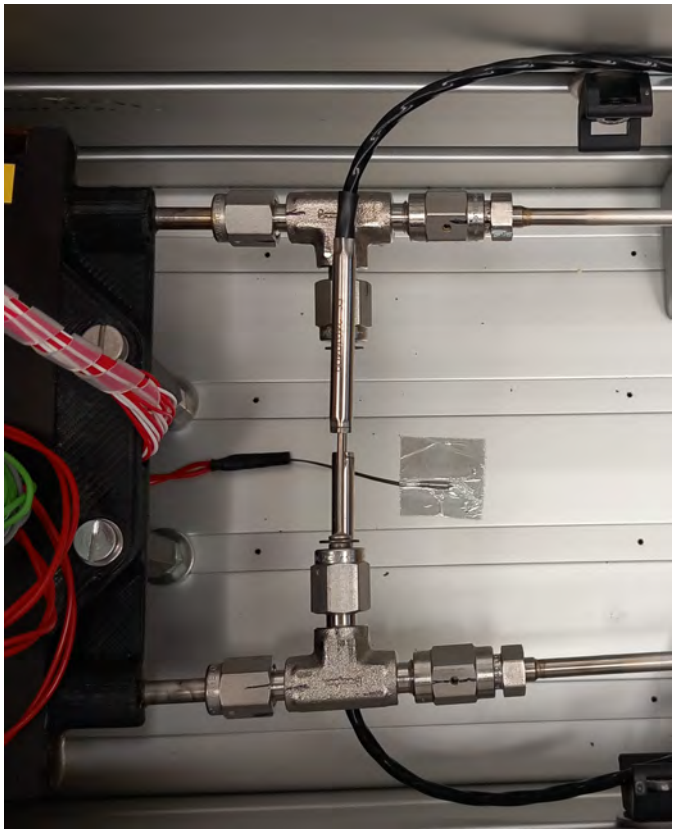

Figure A.3: Photo of the PT100 sensors affixed inside the t-pieces of the CO_2 pipe.

A.2. Systematic uncertainty of the PT100 sensors

In the following, the equation to calculate the systematic uncertainty of the PT100 sensors for each measured temperature can be found.

$$
\begin{aligned}
&R(t) = R0 \cdot (1 + A \cdot t + B \cdot t^2) \qquad (2)\\
&A = 3.9083 \cdot 10^{-3}\,^{\circ}\mathrm{C}^{-1}\\
&B = -5.775 \cdot 10^{-7}\,^{\circ}\mathrm{C}^{-2}\\
&R0 = 200\,\Omega
\end{aligned}
$$

Equation 2: Equation to calculate the systematic uncertainty of the PT100 sensors.

A.3. Heat distribution of the mini-TEDD structure in two configurations

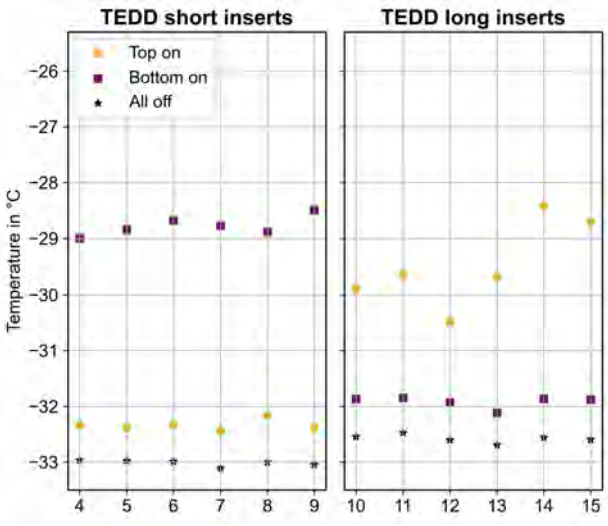

Figure A.4: Values of the temperature sensors of the inserts within the cooling structure for all real and emulated modules on the top side powered in yellow and the bottom side powered in purple. The temperature values when everything is turned off are shown in black. The ambient and CO_2 temperature are adjusted to the thermal runaway curve point with a CO_2 temperature of −33.9 °C and 5.8 W full module power.

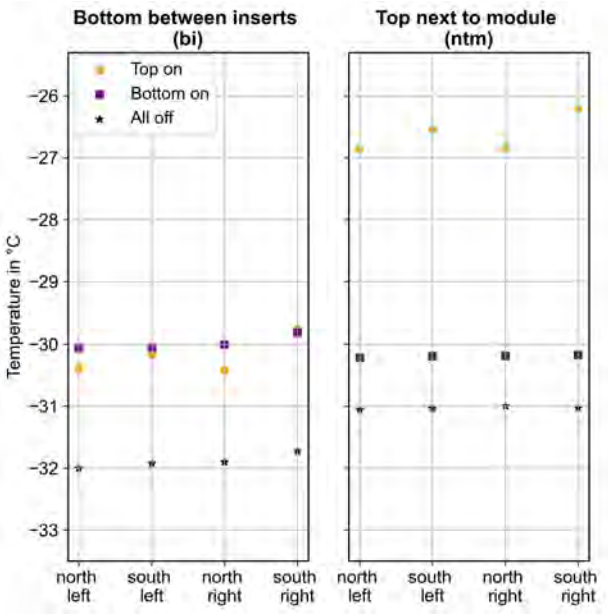

Figure A.5: Values of the temperature sensors mounted on the carbon fiber surface of the cooling structure for all real and emulated modules on the top side powered in yellow and the bottom side powered in purple. The temperature values when everything is turned off are shown in black. The ambient and CO_2 temperature are adjusted to the thermal runaway curve point with a CO_2 temperature of −33.9 °C and 5.8 W full module power.

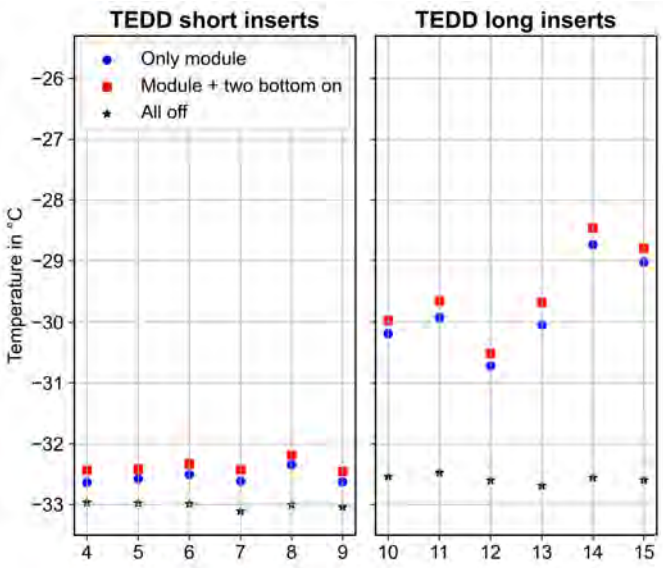

Figure A.6: Values of the temperature sensors of the inserts within the cooling structure for the 2S module on the top center position activated in blue, and with two additional bottom modules powered on the left and right in red. The temperature values when everything is turned off are shown in black. The ambient and CO_2 temperature are adjusted to the thermal runaway curve point with a CO_2 temperature of $-33.9\,°C$ and $5.8\,W$ full module power

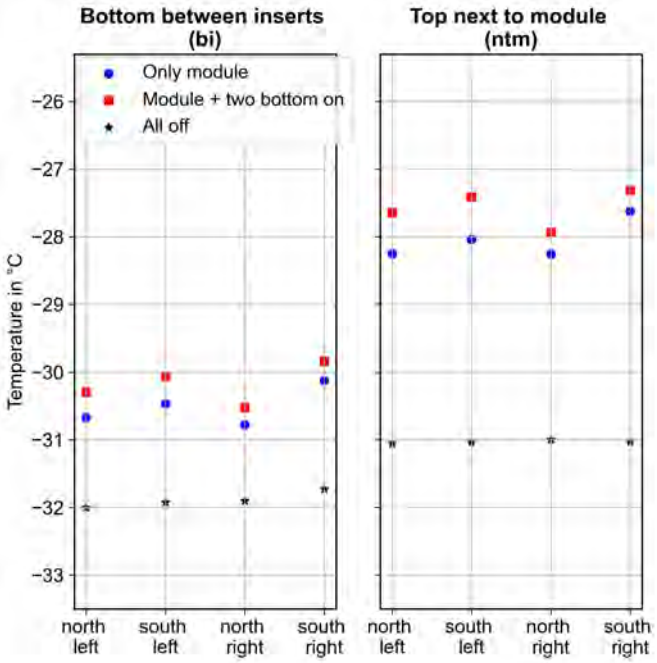

Figure A.7: Values of the temperature sensors mounted on the carbon fiber surface of the cooling structure for the 2S module on the top center position activated in blue, and with two additional bottom modules powered on the left and right in red. The temperature values when everything is turned off are shown in black. The ambient and CO_2 temperature are adjusted to the thermal runaway curve point with a CO_2 temperature of $-33.9\,°C$ and $5.8\,W$ full module power.

Danksagung

An dieser Stelle möchte ich zunächst Prof. Dr. Lutz Feld für die Möglichkeit danken, meine Bachelorarbeit in dieser Arbeitsgruppe zu verfassen, sowie für die zahlreichen Anregungen und Hinweise aus den wöchentlichen Meetings. Ebenso bin ich sehr dankbar für die Gelegenheit, an der Tracker Woche am CERN teilzunehmen.
Des Weiteren möchte ich Prof. Dr. Oliver Pooth für die Übernahme der Zweitkorrektur dieser Arbeit danken.
Ein großer Dank gilt auch Dr. Katja Klein für das Korrekturlesen meiner Arbeit und die hervorragende Betreuung während der gesamten Zeit.
Ein besonderer Dank geht an Vanessa Oppenländer für die ausführliche Einführung in das CO_2 Setup, die geduldige Beantwortung zahlreicher Fragen und die Begleitung bei den thermischen Messungen. Ebenso möchte ich mich für die Bereitstellung der Messdaten für die Thermal Runaway Kurve auf kurzen Inserts bedanken.
Vielen Dank auch an Nicolas Röwert, vor allem für die ausführlichen Diskussionen der Messungen des Wärmeflusses und die Bereitstellung der thermischen Simulationsdaten.
Mein Dank gilt der gesamten Arbeitsgruppe für die angenehme Arbeitsatmosphäre.
Dr. Martin Lipinski danke ich besonders für die Beantwortung aller Fragen zum CO_2 Setup und dem dazugehörigen LabView Programm, sowie Alexander Pauls für die Erklärungen im Bereich Wire-bonding.
Auch Michael Wlochal und Clara Ebisch möchte ich für ihre Unterstützung im mechanischen Bereich, beim Umbau des CO_2 Setups und dem Einbau der PT100 Sensoren danken.
Zuletzt möchte ich meiner Familie und meinen Freunden für ihre ganze Unterstützung und das fleißige Korrekturlesen danken.